Lanthanide speciation in potential SANEX and GANEX actinide/lanthanide separations using tetra-N-donor extractants

Daniel M. Whittaker,[†] Tamara L. Griffiths,[†] Madeleine Helliwell,[‡] Adam N. Swinburne,[†] Louise S. Natrajan,[†] Frank W. Lewis,[‖] Laurence M. Harwood,[‖] Stephen A. Parry[§] and Clint A. Sharrad*[†#⊥]*

[†] Centre for Radiochemistry Research, School of Chemistry, The University of Manchester, Oxford Road, Manchester, M13 9PL, U.K.; [‡] School of Chemistry, The University of Manchester, Oxford Road, Manchester, M13 9PL, U.K; [‖]Department of Chemistry, University of Reading, Whiteknights, Reading, RG6 6AD, U.K.; [§] Diamond Light Source Ltd, Diamond House, Harwell Science and Innovation Campus, Didcot, Oxfordshire, OX11 0DE, U.K.; [#] School of Chemical Engineering and Analytical Science, The University of Manchester, Oxford Road, Manchester, M13 9PL, U.K.; [⊥] Research Centre for Radwaste and Decommissioning, Dalton Nuclear Institute, The University of Manchester, Oxford Road, Manchester, M13 9PL, U.K.

RECEIVED DATE (to be automatically inserted after your manuscript is accepted if required according to the journal that you are submitting your paper to)

TITLE RUNNING HEAD: Lanthanide speciation with N-donor extractants

Abstract

A series of lanthanide(III) complexes with nitrogen donor extractant molecules, that exhibit potential for the separation of minor actinides from lanthanides in the management of spent nuclear fuel, have been directly synthesized and characterized in both solution and solid states. Crystal structures of Pr^{3+}, Eu^{3+}, Tb^{3+} complexes of $CyMe_4$-BTPhen (2,9-bis(5,5,8,8-tetramethyl-5,6,7,8-tetrahydro-1,2,4-benzotriazin-3-yl)-1,10-phenanthroline) and $CyMe_4$-BTBP (2,9-bis(5,5,8,8-tetramethyl-5,6,7,8-tetrahydro-1,2,4-benzotriazin-3-yl)-2,2'-bypyridine) were obtained. The Yb^{3+} complex of $CyMe_4$-BTPhen was also characterized by single crystal X-ray diffraction. The vast majority of these structures displayed the coordination of two of the tetra-N donor extractant ligands to each Ln^{3+} ion, even when in some cases the syntheses were performed with equimolar amounts of lanthanide and N-donor ligand. The structures showed that generally the lighter lanthanides had their coordination spheres completed by a bidentate nitrate ion giving a +2 charged complex cation, whereas the structures of the heavier lanthanides displayed tricationic complex species with a single water molecule completing their coordination environments. Electronic absorption spectroscopic titrations showed the formation of the 1:2 Ln^{3+}:$L_{N4\text{-donor}}$ species (where Ln = Pr^{3+}, Eu^{3+}, Tb^{3+}) in methanol solution when the N-donor ligand was in excess. When the Ln^{3+} ion was in excess, evidence for the formation of a 1:1 Ln^{3+}:$L_{N4\text{-donor}}$ complex species was observed. Luminescent lifetime studies of mixtures of Eu^{3+} with excess $CyMe_4$-BTBP and $CyMe_4$-BTPhen in methanol and applying the Horrock's equation gave consistent q values of ~0.3, indicating that the nitrate coordinated species is dominant in solution. X-ray absorption spectra of the Eu^{3+} and Tb^{3+} species, formed by extraction from an

acidic aqueous phase into an organic phase consisting of an excess of N-donor extractant in pure cyclohexanone or 30 % TBP (tri-*n*-butyl phosphate) in cyclohexanone. The presence of TBP in the organic phase did not alter Ln speciation in the organic phase. Simulation of the EXAFS (Extended X-ray absorption fine structure) region of the spectra, using chemical models established by crystallography and electronic solution spectroscopy, showed the dominant Ln species in the bulk organic phase was a 1:2 Ln^{3+}:$L_{N\text{-donor}}$ species with a nitrate ion completing the coordination sphere giving a dicationic complex species.

KEYWORDS. Separations, Lanthanides, Solvent extraction, Speciation

Introduction

Organic molecules that can selectively coordinate An (actinides) over Ln (lanthanides) are of great interest to the nuclear sector due to their applicability for partitioning in the 'back-end' of the nuclear fuel cycle.[1,2] This interest is due to the fact that if the Ln can be separated from the SNF (Spent Nuclear Fuel) this will make the possibility of transmutation of the long-lived An ions much more accessible.[3] Transmutation is the process of changing one atom into another through nuclear reactions. In this case it would entail isolating the An species and placing in a high neutron flux in order to initiate fission, thereby forming short-lived nuclides that present less of a radiological issue. The necessity to selectively extract the An ions is due to the high neutron absorption cross-sections of the Ln ions which would both decrease the flux in a reactor and create more activation products thereby making transmutation a less attractive option.[4] As

such, work has been continuing for many years into different ligand classes that can perform this separation.

TBP (Tri-*n*-Butyl Phosphate) is the current choice in the UK industry for partitioning U and Pu from the fission products, including the lanthanides.[5] It is used in the PUREX (Plutonium and URanium EXtraction) process and is an efficient ligand for the recovery of Pu(IV) and U(VI) from SNF.[5] However, many different ligand systems have been developed by many different groups in the field of partitioning. The DIAMEX (DIAMide EXtraction) process has been developed by the French Commissariat à l'Energie Atomique (CEA) utilising N'N'-dimethyl-N,N'-dioctylhexylethoxymalonamide (DMDOHEMA) for the recovery of An from HAR (Highly Active Raffinate).[6] The TRUEX (TRansUranic EXtraction) process is an addendum to the PUREX process. The addition of octyl(phenyl)-N,N-di*iso*butylcarboylmethlyphosphineoxide (CMPO) to the PUREX process allows Am and Cm to be extracted alongside U and Pu, so that partitioning and transmutation can be performed on the extracted material thereby lowering the activity of the waste for disposal and therefore the design lifetime of the repository.[7]

The SANEX (Selective ActiNide EXtraction) process aims to separate the minor actinides Am and Cm from the lanthanide fission products. The N-donor extractant $CyMe_4$-BTBP (2,9-bis(5,5,8,8-tetramethyl-5,6,7,8-tetrahydro-1,2,4-benzotriazin-3-yl)-2,2'-bypyridine; Fig. 1) has been shown to exhibit potential for use in SANEX separations.[8] However, the kinetics for actinide extraction with $CyMe_4$-BTBP are relatively slow, so the addition of a phase transfer catalyst is necessary (e.g. DMDOHEMA) if this extractant is to be used for large-scale partitioning.[8] In an attempt to improve the kinetics of extraction with these tetradentate N-donor extractants, greater conformational rigidity was enforced in the ligand backbone with the synthesis of $CyMe_4$-BTPhen (2,9-bis(5,5,8,8-tetramethyl-5,6,7,8-tetrahydro-1,2,4-benzotriazin-3-yl)-1,10-phenanthroline; Fig. 1).[9] This rigid ligand displayed extremely high separation factors

for Am over Eu (68 – 400) which are approximately two orders of magnitude greater than those for $CyMe_4$-BTBP, and exhibited significantly faster kinetics of extraction compared to $CyMe_4$-BTBP.[9]

The GANEX (Group ActiNide EXtraction) process is proposed to separate all of the actinides, in the varying oxidation states, concurrently from the remaining fission products, including the lanthanides. A number of different extractant combinations have been shown to have potential for such a process including $CyMe_4$-BTBP and TBP.[10]

The N-donor extractants, $CyMe_4$-BTPhen and $CyMe_4$-BTBP have demonstrated an enhanced ability to partition SNF mixtures, in particular the separation of minor actinides from the lanthanides.[8,9] However, the mode of action of these ligands with lanthanides and actinides in extraction conditions has not been definitively established. We have used X-ray absorption spectroscopy (XAS) to probe lanthanide (Eu, Tb) species which have been extracted into the organic phase in a series of proposed SANEX and GANEX separations that use $CyMe_4$-BTPhen and $CyMe_4$-BTBP. The EXAFS of the Ln L_{III}-edge spectra obtained from each of these systems has been fitted and compared to the relevant solid state structures obtained by the direct synthesis of Ln^{3+} complexes with these N-donor extractants. The solution state behaviour of the directly synthesized Ln^{3+} complexes in organic solutions has also been studied by UV-visible absorption and luminescence spectroscopies.

Results and Discussion

Synthesis

Lanthanide(III) complexes of the extractant $CyMe_4$-BTPhen were readily synthesized by the addition of $Ln(NO_3)_3$ (Ln = Pr, Eu, Tb, Yb) in acetonitrile to a molar equivalent of $CyMe_4$-BTPhen in dichloromethane (DCM). The reaction solution was allowed to evaporate to dryness

leaving a powdered residue that could be crystallised from a mixture of CH_3CN, DCM and ethanol. In all examples, yellow crystals were obtained. Elemental analysis, single crystal XRD (X-ray diffraction; see Solid state structure section) and ESI (electrospray ionisation – positive ion) mass spectrometry indicated that in the majority of cases complex cations of stoichiometry 1:2 Ln^{3+}:$CyMe_4$-BTPhen with nitrate counter ions were obtained even though the syntheses were conducted with equimolar amounts of $Ln(NO_3)_3$ and $CyMe_4$-BTPhen. The only exception was found during the synthesis of the Pr^{3+} complex of $CyMe_4$-BTPhen where the majority product was still consisted of a 1:2 Pr: $CyMe_4$-BTPhen complex cation but with a $[Pr(NO_3)_5]^{2-}$ counter ion present per cationic unit. Initial crystallisation of this mixture was able to isolate a small amount of the same cationic species with only nitrate present as counterions, as determined by XRD (see Solid state structure section). The structural determinations show that the Ln^{3+} coordination sphere is completed by a single nitrate anion for the Pr^{3+} complexes (**1**, **2**), whilst for the Eu^{3+}, Tb^{3+} and Yb^{3+} complexes (**3-5**) a single molecule of water completes the coordination sphere (see Solid state structure section). However, ESI mass spectrometry of all the studied Ln^{3+} complexes with $CyMe_4$-BTPhen from methanol solution indicate that a nitrate ion is coordinated and there was no evidence to suggest a water molecule was present in the coordination sphere.

The synthesis of Ln^{3+} complexes (Ln = Pr, Eu, Tb) of $CyMe_4$-BTBP was also attempted by adding a dichloromethane solution of the ligand to ½ an equivalent of $Ln(NO_3)_3$ in methanol. The powdered product obtained on evaporation of the reaction mixture was crystallised by slow evaporation from a mixture of toluene, isopropanol, ethanol and dichloromethane. Characterisation of the bulk crystallised material obtained from all the attempted Ln^{3+} complexations of $CyMe_4$-BTBP indicated that a mixture of products were present, which is likely to be due to the formation of products with different combinations of Ln^{3+}:$CyMe_4$-BTBP ratios

and anionic molecular ions (i.e. NO_3^-, $[Ln(NO_3)_6]^{3-}$, $[Ln(NO_3)_5]^{2-}$). However, the selection of individual crystals obtained from these reactions was able to afford the structural determination of a number of products by XRD. The vast majority of these structures indicated complex cations of 1:2 Ln^{3+}:$CyMe_4$-BTBP stoichiometry (**6-8, 10**) with nitrates (**6-8**, **10**) and metallonitrates (**7**) present as counter-ions. Previously, the only structures of Ln-BTBP complexes to have been isolated have been with the ligand C2-BTBP (6,6'-bis-(5,6-diethyl-1,2,4-triazin-3-yl)-2,2'-bipyridine) and these had a single C2-BTBP molecule coordinated to the Ln^{3+} ion.[11] It was noted that in solution both 1:1 and 1:2 Ln^{3+}:C2-BTBP complexes were observed.[11] Our attempts to form the Eu^{3+} complex of $CyMe_4$-BTBP produced a 1:1 Eu^{3+}:$CyMe_4$-BTBP molecular species (**9**) in addition to the 1:2 Eu^{3+}:$CyMe_4$-BTBP complex cation containing species . The Pr^{3+} and Eu^{3+} complexes isolated in the solid state (**6-9**) have a nitrate ion/s completing the coordination sphere, while only the Tb^{3+} complex of $CyMe_4$-BTBP has a water molecule in its coordination environment. The ESI mass spectra of all the $CyMe_4$-BTBP complexes studied from methanol only indicated $[Ln(CyMe_4\text{-}BTBP)_2(NO_3)]^{2+}$ species were present, as for the $CyMe_4$-BTPhen complexes. This suggests that the 1:2:1 Ln^{3+}:$CyMe_4$-BTBP:NO_3^- complex was dominant in solution, while other compositions were only present in solution in minor quantities, if at all.

Solution spectroscopy

The UV-visible absorption spectra of the complexes **2** – **4,** isolated in a pure bulk form, dissolved in methanol are dominated by charge transfer transitions in the UV region of the spectra (see supporting information). These transitions are most likely due to π-π* transitions from the aromatic nature of the $CyMe_4$-BTPhen ligand. A clear difference in the spectral profile is observed between the free $CyMe_4$-BTPhen ligand and the Ln^{3+} complexes, indicating the electronic structure of the $CyMe_4$-BTPhen molecule is perturbed upon lanthanide(III)

coordination. Essentially no difference is observed between the spectral profiles for **2** – **4** indicating that there is little or no influence by the type of coordinating lanthanide ion on the electronic structure of the $CyMe_4$-BTPhen ligand. The limited solubility of these complexes in most common solvents precluded the study of the typically weakly absorbing *f-f* transitions of the lanthanides in 1 cm pathlength cells.

Titrations of $CyMe_4$-BTPhen and Cy-Me_4-BTBP with the lanthanide ions, Pr^{3+}, Eu^{3+} and Tb^{3+}, in methanol were performed to study the lanthanide speciation behaviour of these extractant molecules, in particular the equilibrium between 1:1 and 1:2 Ln^{3+}:$L_{N4\text{-donor}}$ species. The titrations of $CyMe_4$-BTPhen with each of the lanthanides studied show there is essentially no difference in the titration profiles with different lanthanide ions (see Figure 2 for Pr^{3+} and supporting information). Sharp decreases in the intensity of the absorption maxima for the free Cy-Me_4-BTPhen at 261 and 295 nm with the addition of up to ½ equivalent of $Ln(NO_3)_3$ are observed. The absorption maximum at 261 nm also shifts to ~266 nm with the addition of $Ln(NO_3)_3$. Isobestic points are observed at 229 and 279 nm. Further additions of $Ln(NO_3)_3$, up to 3 equivalents, result in a subtle decrease in the absorption intensity for most of the spectrum but with no changes in the shape of the spectral profile. This indicates that the 1:2 Ln^{3+}:$CyMe_4$-BTPhen complex forms with the initial addition of $Ln(NO_3)_3$, as expected.[11,12] The subtle changes in spectra when more than ½ equivalent of $Ln(NO_3)_3$ are most likely explained by an equilibrium being established between 1:1 and 1:2 Ln^{3+}:$CyMe_4$-BTPhen species, where more 1:1 complex is likely to form with increasing additions of $Ln(NO_3)_3$. Similar behaviour is observed for the titrations of Cy-Me_4-BTBP with $Ln(NO_3)_3$ (see Figure 3 for Eu^{3+} and supporting information). Absorption maxima at 228 and 289 nm sharply decrease in intensity with the initial addition of $Ln(NO_3)_3$ up to ½ equivalents. Two absorption maxima are seen to emerge at 334 and 346 nm with the initial addition of $Ln(NO_3)_3$. Further additions of $Ln(NO_3)_3$ also result in a

subtle decrease in the absorption intensity for most of the spectrum. Therefore, it can be deduced that the 1:2 Ln^{3+}:$CyMe_4$-BTPhen/$CyMe_4$-BTBP complex is probably most favoured to form but the 1:1 species can be forced to form in solution with excess Ln^{3+} ion present. Similar results have been previously observed for Ln^{3+} complexation behaviour with analogous BTBP ligands.[12]

The absorption spectroscopic studies showed no difference between the light and heavy lanthanides, but X-ray diffraction studies (see Solid state structure section) indicate the heavy lanthanides in the 1:2 Ln^{3+}:$CyMe_4$-BTPhen/$CyMe_4$-BTBP complexes prefer to have their coordination sphere completed by water, whereas the lighter lanthanide complexes generally prefer to have nitrate in their coordination environment, a consequence of the lanthanide contraction. This is commonly observed in series of lanthanide complexes of a given multidentate ligand.[13] Luminescence studies were therefore undertaken in an attempt to assess the involvement of nitrate and water in the coordination sphere of these lanthanide species. Excitation and emission spectra of the Eu^{3+} and Tb^{3+} complexes with $CyMe_4$-BTPhen and $CyMe_4$-BTBP are displayed in Figure 4 and in the supplementary information. Excitation into the intra-ligand absorption bands (280 – 330 nm) of the Eu^{3+} and Tb^{3+} complexes produced characteristic *f*-centered emission spectra with resolvable bands due to the $^5D_0$ to ^7F_J and $^5D_4$ to ^7F_J (J = 0 to 6) transitions respectively. The emission spectrum of the Eu^{3+} complexes are dominated the electric dipole allowed $\Delta J = 2$ transition, which is hypersensitive to site symmetry; the absence of hyperfine structure in this band indicates that the complexes exist as a single emissive species on the experimental timescale.[14] The respective excitation spectra recorded at the emission maxima (545 nm for Tb^{3+} and 616 nm for Eu^{3+}) display ligand centered absorption bands that overlap well with the absorption spectra indicating that sensitised emission is occurring in all the systems under study.

In order to assess the inner coordination sphere of the complexes, lifetime data were recorded in MeOH and d_4-methanol following 320 nm excitation and the number of coordinated methanol molecules determined according to the Horrock's equation (Equation 1):

$$q_{Bound\ MeOH} = A\left[\left(\frac{1}{\tau_{MeOH}}\right) - \left(\frac{1}{\tau_{CD_3OD}}\right)\right] \quad (1)^{15}$$

where A is a proportionality constant; A = 2.1 ms for Eu^{3+} and A = 8.4 ms for Tb^{3+}.

For solutions of Eu^{3+} and $CyMe_4$-BTPhen in a 2:1 molar ratio, this gave a q value of 0.3; an identical q value was obtained for the analogous complex with $CyMe_4$-BTBP of 0.3 (Table 1). This strongly suggests that the first coordination sphere of the complexes is completed by ligation of nitrate anions rather than exchangeable solvent molecules and there may be a minor species that exists with either water or methanol occupying this coordination site for these Eu^{3+} complexes. Since the emissive quantum yield of a solvated species would be much lower, the contribution to the initial emission intensity will be low, perhaps precluding observation of a second species in solution and/or the rate of solvent and nitrate anion exchange is much faster than the luminescence timescale so a non-integer value of q is determined. Similar data were obtained for 1:3 and 1:5 molar ratios of Eu^{3+} with both N_4-donor ligands, and the isolated complexes **3** and **8**, suggesting that the 1:2 Ln^{3+}:$L_{N4\text{-donor}}$ complex is the only emissive species formed under these conditions.

In the case of the Tb^{3+} complexes of both ligands, excitation into the ligand absorption bands resulted in comparatively weak emission spectra. This is unsurprising given the estimated triplet energies of the ligands and the high energy emissive $^5D_4$ excited state and suggests that back energy transfer from the Tb^{3+} excited manifold to the ligand triplet state is a competitive non-radiative decay process.[16] This is corroborated by the fact that the radiative lifetimes for the Tb^{3+} emission are extremely short; the kinetic traces could be satisfactorily fitted with two

exponential functions giving lifetime values of approximately 18 and 6 μs (for solutions of BTBP in MeOH). Moreover, the kinetic traces recorded without a time gate and delay additionally exhibit a short lived component of nanosecond order, which we attribute to ligand centered emission.

Solid state structure

Single crystal X-ray diffraction studies of the complexes of Tb^{3+}, Eu^{3+} and Pr^{3+} with the ligands $CyMe_4$-BTBP and $CyMe_4$-BTPhen were obtained (**1** – **4**, **6** – **10**). The complex of Yb^{3+} with $CyMe_4$-BTPhen was also studied (**5**). Plots of these structures are displayed in Figures 6 – 10 (complexes **1**, **3**, **8** – **10**) and supporting information (complexes **2**, **4**-**7**) with crystal data given in Tables 2 and 3. In the vast majority of cases (**1** – **8** and **10**), two of the N-donor ligands (either $CyMe_4$-BTBP or $CyMe_4$-BTPhen) were found to coordinate to the metal centre occupying four coordination sites each with another ligand (water or nitrate) occupying a cavity between the two bound N-donor ligands giving a distorted capped square antiprismatic geometry about the Ln^{3+} centre. This leads to a total coordination number of nine for water coordinated complexes (**3** – **5**, **10**) and ten for the bidentate nitrate coordinated complexes (**1**, **2**, **6** – **8**).

For the Ln^{3+} complexes with $CyMe_4$-BTPhen, only 1:2 Ln^{3+}:$L_{N4\text{-}donor}$ coordination stoichiometries have been isolated and structurally characterized in the solid state. The nitrate ion is found to occupy the remaining coordination sites in the Pr^{3+} complexes isolated while a single water molecule completes the coordination sphere for the $CyMe_4$-BTPhen complexes of the heavier Ln^{3+} ions investigated in this study ($Eu^{3+,}$ Tb^{3+} and Yb^{3+} in **3** – **5**). This is likely to be due to a combined effect of the lanthanide contraction and the structural rigidity of the $CyMe_4$-BTPhen ligand sterically hindering the remaining coordination site/s in the more contracted structures of Eu^{3+}, Tb^{3+} and Yb^{3+} such that only water can access this binding cavity

in these solid state systems. However, previous work has shown that the 1:2 complex of Eu^{3+}:$CyMe_4$-BTPhen can be obtained with a nitrate ion completing the coordination sphere in the solid state where methanol was used as the reaction solvent.[9] Thus, indicating that the position of the equilibrium between bound nitrate and bound water in these Ln^{3+} complexes may be influenced by the choice of solvent. The nitrate coordinated complexes form +2 charged complex cations while the water coordinated complexes form tricationic complex cations, where charge balance is achieved with non-binding nitrate anions in the crystal lattice (**1**, **3** – **5**) or with an anionic metallonitrato species (**2**). The previously obtained $[Eu(CyMe_4\text{-}BTPhen)_2(NO_3)]^{2+}$ solid-state complex was also charged balanced with pentanitrato lanthanide anionic molecule.[9] Complexes **3 - 5** are isostructural crystallising in the orthorhombic Fdd2 space group.

All the M-N bond lengths in the $CyMe_4$-BTPhen containing structures decrease as the lanthanide series is traversed from left to right (Table 4), as expected due to the lanthanide contraction. In all cases, the lanthanide ion sits outside of the plane of the N-donor ligand cavity. The out-of-plane displacement of the Ln^{3+} ion from the average plane defined by the four coordinating nitrogens for each N-donor ligand follows a similar trend to the bond lengths by decreasing across the lanthanide series; ~ 0.80/0.71, 0.77/0.62, 0.56, 0.55 and 0.51 Å for species **1** – **5**, respectively. The average M-$N_{triazinyl}$ bonds lengths are consistently longer than those for the M-N_{Phen} bonds in the Eu^{3+}, Tb^{3+} and Yb^{3+} complexes (**3-5**). This may imply a greater degree of interaction exists between the Ln^{3+} ion and the phenanthroline N-donors than that with the triazinyl N-donors. However the same cannot be said for the structures of the Pr^{3+} complexes obtained (**1**,**2**) where in some instances the M-N_{Phen} bond lengths are in fact longer than the M-$N_{trazinyl}$ bond distances. The previously obtained structure of $[Eu(CyMe_4\text{-}BTPhen)_2(NO_3)]^{2+}$ shows little difference between the Eu-$N_{triazinyl}$ and Eu-N_{Phen} bond distances.[9] Therefore, it is most likely the triazinyl groups are restrained to be further away from the Ln^{3+} centre relative to

the phenanthroline backbone as the Ln centre approaches the plane of the $CyMe_4$-BTPhen binding cavity, as this is only evident for the latter lanthanides. The Ln-O_{water} bond distances also decrease as the lanthanide series is traversed from left to right due to the lanthanide contraction (Table 3). The Pr-$O_{nitrate}$ bond distances for **1** and **2** (2.592(8), 2.542(8) Å for **1**; 2.581(4), 2.604(5) Å for **2**) are typical for Pr^{3+} complexes with coordinated nitrates (2.5 – 2.8 Å).[11, 17,18]

Where $CyMe_4$-BTBP is the ligand, both 1:1 (**9**) and 1:2 Ln^{3+}:$CyMe_4$-BTBP (**6** – **8**, **10**) coordination structures were isolated. Structures of metal complexes with $CyMe_4$-BTBP have only been previously obtained for Eu^{3+}, U^{4+} and $\{UO_2\}^{2+}$.[19,20]. Previous studies of the complexation of Eu^{3+} with $CyMe_4$-BTBP, using a similar preparation described in this work, isolated structures consisting of the same 1:2 and 1:1 Eu^{3+}:$CyMe_4$-BTBP complex species found structures **8** and **9**, respectively, but in different crystal forms due to either different counter ions or alternate solvent molecules of crystallization present in the lattices. Further structural information has been obtained for Ln^{3+} complexes with C2-BTBP where only 1:1 Ln:C2-BTBP complexes were isolated essentially for the entire lanthanide series.[11] The remaining coordination sites were occupied by three nitrate anions to give charge neutral species.[11] The structure of the europium(III) complex **9** is analogous to these Ln complexes of C2-BTBP. For the cationic Ln complexes of $CyMe_4$-BTBP charge balance was achieved either with extra lattice nitrate anions (**6**, **8** and **10**) or in combination with a hexanitratometallo anion (**7**). The two crystalline forms obtained from the complexation of Eu^{3+} with $CyMe_4$-BTBP offers further insight into the equilibrium between 1:1 and 1:2 Ln:BTBP/BTPhen complex stoichiometries. Although, it may be possible for both these stoichiometries to be isolated the vast majority of the structural evidence indicates that the lanthanides prefer to coordinate to two of these class of tetra-N donor extractants, wherever possible. In contrast to the $CyMe_4$-BTPhen structures, metal bound nitrate ions are observed with all $CyMe_4$-BTBP species except Tb^{3+}. This is presumably due to the

greater flexibility afforded from the bipyridine, compared to the 'locked' phenanthroline, permitting the sterically larger bidentate nitrate anion, relative to water, to bind the Ln^{3+} centre.

For all the complexes of $CyMe_4$-BTBP (**6**-**10**), the Ln-N bond distances (Table 5) decrease as the lanthanides series is progressed from left to right, similar to the $CyMe_4$-BTPhen and C2-BTBP containing structures.[11] The Ln-$O_{nitrate}$ bond lengths also clearly decrease across the series demonstrating the lanthanide contraction again. The 1:2 Ln^{3+}:$CyMe_4$-BTBP complexes bear further similarity to those of $CyMe_4$-BTPhen with the Ln^{3+} ion located outside of the average plane of the tetra-N donor cavity and this displacement following the same trend as the bond lengths, decreasing across the series; ~ 0.73/0.78, 0.72/0.76, 0.69 and 0.56 Å for **6**, **7**, **8**, and **10**, respectively. However, the 1:1 Eu^{3+}:$CyMe_4$-BTBP complex (**9**) does effectively sit in the plane average plane of the four N-donor atoms (out-of plane displacement ~ 0 Å). In contrast to the $CyMe_4$-BTPhen structures, there is no clearly identifiable trend between the M-N_{bipy} and M-$N_{triazinyl}$ bond lengths for all the $CyMe_4$-BTBP complexes. This suggests the greater flexibility of the bipyridyl group, relative to the phenanthroline group, allows minimal distinction between the triazinyl nitrogens and the bipyridyl nitrogens when coordinated to a Ln^{3+} ion.

X-ray absorption spectroscopy of Ln extracted species

X-ray absorption spectra were obtained for Eu^{3+} and Tb^{3+} species formed by extraction from an acidic aqueous phase into an organic phase containing an excess of either $CyMe_4$-BTBP or $CyMe_4$-BTPhen in cyclohexanone as a guide for speciation in a potential SANEX process. Studies were also performed for potential GANEX-like systems where the organic phase also included 30 % TBP. X-ray absorption spectra were obtained for the crystallographically characterized solids, $[Eu(CyMe_4\text{-BTPhen})_2(H_2O)]^{3+}$ (**3**) and $[Tb(CyMe_4\text{-BTPhen})_2(H_2O)]^{3+}$ (**4**), for comparative purposes. The spectra obtained show little difference between the extracted

species with or without the presence of TBP (Figures 11, 12 and supporting information). Therefore, indicating that the presence of TBP does not influence lanthanide speciation when used in a potential GANEX process with $CyMe_4$-BTBP or $CyMe_4$-BTPhen. The XAS profiles for the directly synthesized solid species (**3**, **4**) also correlate well with the corresponding extracted species (Figures 11, 12) suggesting that the $[Ln(CyMe_4\text{-}BTPhen)_2(H_2O)]^{2+}$ coordination species found in the solid state also exists in the bulk organic phase after extraction.

Simulation of the EXAFS (Extended X-ray absorption fine structure) data for all samples was performed using models derived from lanthanide complexes with two coordinating N_4-donor ligands (either $CyMe_4$-BTBP or $CyMe_4$-BTPhen, where appropriate) and water or nitrate occupying the remaining coordination site/s, as indicated by the solid and solution state characterisation of the directly synthesized complexes. The simulations show that for all samples the inclusion of a nitrate ion, instead of water, in the lanthanide coordination sphere give the best fits (Tables 6 & 7, Figure 13 and supporting information). For each sample, the immediate lanthanide coordination environment is best modelled with two shells: an oxygen shell with an occupancy of two corresponding to a bidentate bound nitrate ion, and a nitrogen shell with an occupancy of eight from the two coordinated N_4-donor ligands. The fits for all the Eu L_{III}-edge data (Table 6) show the first oxygen shell to be located between 2.34 and 2.44 Å from the Eu^{3+} centre when modelled as nitrate which is shorter than the Eu-$O_{(nitrate)}$ bond lengths determined for structures **8** (2.56(1) Å) and **9** (2.548(4) Å) but still falls within the range of all known Eu-$O_{(nitrate)}$ distances (2.31 – 2.82 Å) established by crystallography.[17,21] The oxygen shells for all the Tb L_{III} edge EXAFS spectra modelled with nitrate (Table 7) are located at similar distances (2.32 – 2.39 Å) from the Ln centre, as those for the Eu samples. These Tb-O distances fall within the relatively wide range of known Tb-$O_{(nitrate)}$ bond lengths (2.19 – 2.85 Å),[17,22] but only a relatively small number of structures exhibit Tb-$O_{(nitrate)}$ distances within the range observed by EXAFS in

these studies.[17,23] The first N shell of eight atoms is found at ~2.55 and 2.52 Å for the Eu and Tb samples, respectively, which is in agreement with the Ln-N bond lengths of Eu complexes (**3**, **8**, **9**: 2.50 – 2.58 Å) and Tb complexes (**4**, **10**: 2.42 – 2.52 Å) determined by XRD. The inclusion of further shells outside of the immediate coordination environment was found to significantly improve the fits of the EXAFS data. The best fits for all samples were obtained using a nitrogen shell of a single atom located at ~3.02 and 2.93 Å from the Ln centre for Eu and Tb samples, respectively, due to the coordinated nitrate, and three carbon shells at distances from the Ln^{3+} (Eu^{3+}, Tb^{3+}) ion of 3.4 – 3.5, 4.45 – 4.55 and 4.9 – 5.0 Å due to the carbon backbone of the tetradentate ligands. The location of the nitrate N shell and the closest C shell to the Ln centre are in close agreement to those distances found in the structurally characterized complexes of **3**, **4**, **8** - **10** (Eu-$N_{nitrate}$ ~ 3.0, Ln-C ~ 3.4 Å).[24] The distances of the two outer carbon shells from the Ln^{3+} ion used to fit the EXAFS data (Ln-C ~ 4.5, 4.9 Å) do not correlate to the those distances found in the corresponding X-ray crystal structures (Ln-C ~ 4.7, 5.3 Å).[25] This suggests that either these outer carbon shells are averaged in the EXAFS possibly influenced by multiple scattering effects, or fluctuation of the N_4-donor ligand occurs in these lanthanide complexes under the conditions studied. The variations of the occupancies of the carbon shells from the Eu L_{III} edge data of the $CyMe_4$-BTBP containing systems (Table 6) gives further evidence to that at least the $CyMe_4$-BTBP ligand fluctuates when coordinated to the Eu^{3+} ion.

The EXAFS simulations of complexes **3** and **4** (Table 6 & 7) clearly show better fits when the nitrate ion is included in the coordination sphere even though the structures determined by XRD definitively show that a water molecule is coordinated to the Ln^{3+} ion. Luminescence spectroscopy and mass spectrometry also provide evidence that the nitrate ion completes the Ln^{3+} coordination sphere. Therefore, it is likely that crystals selected for XRD, where water was found to bind to the Ln, are not a true reflection of the bulk product obtained in these syntheses. The

EXAFS of the bulk products from the preparation of **3** and **4** were simulated with water coordinated to the Ln^{3+} ion giving Ln-O distances (**3** – 2.29 Å, **4** – 2.25 Å) that are substantially shorter than those obtained by crystallography (**3** – 2.414(6) Å, **4** – 2.397(6) Å) and just fall outside the range of Ln-O_{water} bond lengths from all previously reported structures (Eu-O_{water}: 2.27 – 2.72 Å; Tb-O_{water}: 2.27 – 2.70).[17,26] Hence, it most likely that majority product obtained from these synthetic procedures has two of the N_4-donor ligands bound to the lanthanide with nitrate ion, rather than a water molecule, completing the coordination environment.

Experimental

General

Elemental analyses were performed using a Carlo ERBA Instruments CHNS-O EA1108 elemental analyser was used for C, H and N analyses and a Fisons Horizon elemental analysis ICP-OES spectrometer for Pr, Eu and Tb analyses. Electrospray ionisation (positive ion) mass spectrometry was performed using a Micromass Platform spectrometer. Solution UV-vis spectra were recorded on a PG Instruments T60U spectrophotometer with a fixed spectral bandwidth of 2 nm. Typical scan ranges were 200-500 nm at a scan rate ~390 nm min^{-1} Excitation and emission spectra were recorded with Edinburgh Instrument FP920 phosphorescence lifetime spectrometer equipped with a 5 watt microsecond pulsed xenon flashlamp (with single 300 mm focal length excitation and emission monochromators in Czerny Turner configuration) and a red sensitive photomultiplier in peltier (air cooled) housing, (Hamamatsu R928P) using a gate time of 0.05 ms and a delay time of 0.5 ms. Excitation spectra were obtained using the following emission wavelengths: Eu^{3+} - 616 nm; Tb^{3+} - 545 nm. Lifetime data were recorded following 320 nm excitation with microsecond pulsed xenon flashlamp (Edinburgh Instruments), using the multi-channel scaling method. Lifetimes were obtained by tail fit on the data obtained, and

quality of fit judged by minimization of reduced chi-squared and residuals squared. Where the decay profiles are reported as monoexponential, fitting to a double exponential decay yielded no improvement in fit as judged by minimization of residual squared and reduced chi squared.

Syntheses and Solution Preparations

All chemicals were purchased from Sigma Aldrich and were used as supplied. $CyMe_4$-BTPhen and $CyMe_4$-BTBP were synthesized as previously described.[9,11]

Synthesis of Pr^{3+} complexes with $CyMe_4$-BTPhen. A solution of $Pr(NO_3)_3.6H_2O$ (23 mg, 54 μmol) in CH_3CN (5 mL) was added to a solution of $CyMe_4$-BTPhen (30 mg, 54 μmol) in DCM (5 mL) and left stand to evaporate to dryness. The resultant powder was dissolved in a mixture of CH_3CN (2 mL), DCM (2 mL) and EtOH (0.5 mL) and again allowed to slowly evaporate in order to crystallise. A yellow plate-like crystal was selected from the isolated material and XRD (X-ray diffraction) analysis indicated the composition of the crystal was of the formulation $[Pr(CyMe_4\text{-BTPhen})_2(NO_3)](NO_3)_2.10H_2O$ (**1.**$10H_2O$). Elemental analysis of the isolated material indicated the composition of the bulk product was of the formulation $[Pr(CyMe_4\text{-BTPhen})_2(NO_3)][Pr(NO_3)_5].2H_2O$ (**2**.$2H_2O$). Elemental analysis: Calculated for $[(C_{34}H_{38}N_8)_2(NO_3)Pr][(NO_3)_5Pr].2H_2O$: C, 45.19; H, 4.46; N, 17.05; Pr, 15.59 %. Found: C, 45.01; H, 4.08; N, 16.90; Pr, 15.23 %. The bulk material was dissolved in MeOH (1 mL) and allowed to slowly evaporate over 1 week yielding yellow block-like crystals suitable for single crystal XRD analysis (Yield = 0.03 g). ESI-MS (+ve ion): *m/z* 659 ($[(C_{34}H_{38}N_8)_2(NO_3)Pr]^{2+}$). UV-visible spectrum (MeOH) [λ_{max}/nm (ε_{max}/$Lmol^{-1}cm^{-1}$)]: 266 (71000), 321 (38000).

Synthesis of [Eu(CyMe$_4$-BTPhen)$_2$(H$_2$O)](NO$_3$)$_3$.2H$_2$O (3.2H$_2$O**).** A solution of Eu(NO$_3$)$_3$.6H$_2$O (24 mg, 54 μmol) in CH$_3$CN (5 mL) was added to a solution of CyMe$_4$-BTPhen (30 mg, 54 μmol) in DCM (5 mL) and left to stand to evaporate to dryness. The resultant powder was dissolved in a mixture of CH$_3$CN (2 mL), DCM (2 mL) and EtOH (0.5 mL) and allowed to slowly evaporate yielding yellow block-like crystals suitable for single crystal XRD analysis (Yield = 0.02 g). Elemental analysis: Calculated for [(C$_{34}$H$_{38}$N$_8$)$_2$(H$_2$O)Eu](NO$_3$)$_3$.2H$_2$O: C, 54.11; H, 5.48; N, 17.63; Eu, 10.07 %. Found: C, 54.18; H, 5.07; N, 17.61; Eu, 10.51 %. ESI-MS (+ve ion): *m/z* 666 ([(C$_{34}$H$_{38}$N$_8$)$_2$(NO$_3$)Eu]$^{2+}$). UV-visible spectrum (MeOH) [λ_{max}/nm (ε_{max}/Lmol^{-1}cm^{-1})]: 266 (99000), 321 (52000).

Synthesis of [Tb(CyMe$_4$-BTPhen)$_2$(H$_2$O)](NO$_3$)$_3$.H$_2$O (4.H$_2$O**).** The synthesis was performed as described for **2** except using Tb(NO$_3$)$_3$.5H$_2$O (17 mg, 38 μmol) and CyMe$_4$-BTPhen (21 mg, 38 μmol) as the initial reagents. Yellow plate-like crystals were obtained suitable for single crystal XRD analysis (Yield = 0.02 g). Elemental analysis: Calculated for [(C$_{34}$H$_{38}$N$_8$)$_2$(H$_2$O)Tb](NO$_3$)$_3$.H$_2$O: C, 54.51; H, 5.38; N, 17.76; Tb, 10.61 %. Found: C, 54.69; H, 5.17; N, 17.73; Tb, 9.82 %. ESI-MS (+ve ion): *m/z* 669 ([(C$_{34}$H$_{38}$N$_8$)$_2$(NO$_3$)Tb]$^{2+}$). UV-visible spectrum (MeOH) [λ_{max}/nm (ε_{max}/Lmol^{-1}cm^{-1})]: 265 (96000), 322 (51000).

Synthesis of [Yb(CyMe$_4$-BTPhen)$_2$(H$_2$O)](NO$_3$)$_3$.3H$_2$O (**5**.3H$_2$O). The synthesis was performed as described for **2** except using Yb(NO$_3$)$_3$.5H$_2$O (24 mg, 54 μmol) and CyMe$_4$-BTPhen (30 mg, 54 μmol) as the initial reagents. Yellow rhombohedron-like crystals were obtained suitable for single crystal XRD analysis. Yield < 0.01 g. ESI-MS (+ve ion): *m/z* 677 ([(C$_{34}$H$_{38}$N$_8$)$_2$(NO$_3$)Tb]$^{2+}$).

Synthesis of Ln^{3+} complexes with $CyMe_4$-BTBP. A solution of $CyMe_4$-BTBP (30 mg, 56 µmol) in DCM (1 mL) was added to a solution of $Ln(NO_3)_3.xH_2O$ ($Pr(NO_3)_3.6H_2O$ – 12 mg, 28 µmol, $Eu(NO_3)_3.6H_2O$ – 13 mg, 28 µmol or $Tb(NO_3)_3.5H_2O$ – 12 mg, 28 µmol) in MeOH (1 mL). CH_3CN (1.5 mL) was added to the reaction mixture and the solution was allowed to evaporate to dryness. Once dry, toluene (1.25 mL), EtOH (1.25 mL), ^{i}PrOH (1.25 mL) and DCM (1.25 mL) were added to dissolve the powdered residues and left to stand and allowed to slowly evaporate. Crystals suitable for single crystal XRD were obtained over several weeks. The mixtures afforded a variety of crystals of varying compositions determined by single crystal XRD analysis to be: $[Pr(CyMe_4\text{-}BTBP)_2(NO_3)](NO_3)_2.4MeOH.H_2O$ (**6**.4MeOH.H_2O) $[Pr(CyMe_4\text{-}BTBP)_2(NO_3)]_2[Pr(NO_3)_6](NO_3).6CH_3CN$ (**7**.6CH_3CN), $[Eu(CyMe_4\text{-}BTBP)_2(NO_3)](NO_3)_2.4EtOH.2H_2O$ (**8**.4EtOH.$2H_2O$), $[Eu(CyMe_4\text{-}BTBP)(NO_3)_3]$.toluene (**9**.toluene) and $[Tb(CyMe_4\text{-}BTBP)_2(H_2O)](NO_3)_2.4EtOH$ (**10**.4EtOH). Bulk analysis of the crystallised samples by ESI-MS provided the following data:- ESI-MS (+ve ion): *Pr^{3+} complexation - m/z* 635 ($[(C_{32}H_{38}N_8)_2(NO_3)Pr]^{2+}$); *$Eu^{3+}$ complexation - m/z* 641 ($[(C_{32}H_{38}N_8)_2(NO_3)Eu]^{2+}$); *$Tb^{3+}$ complexation - m/z* 643 ($[(C_{32}H_{38}N_8)_2(NO_3)Tb]^{2+}$).

Solution preparation for UV-visible spectroscopic studies of Ln^{3+} complexation with $CyMe_4$-BTPhen and $CyMe_4$-BTBP. Methanolic solutions of the ligands, $CyMe_4$-BTBP and $CyMe_4$-BTPhen, (1×10^{-4} M, 0.4 mL) were added to a quartz cuvette of 1 cm pathlength and the solutions were diluted to 2 mL with MeOH (2×10^{-5} M). At this point an initial spectrum of the ligand was recorded. Metal solutions of $Eu(NO_3)_3.6H_2O$, $Pr(NO_3)_3.6H_2O$ and $Tb(NO_3)_3.5H_2O$ (4×10^{-4} M) in MeOH were used. For each titration, the metal solution was added into the cuvette in 10 µL (4×10^{-9} mol; 0.1 equivalent) aliquots, shaken and spectra recorded after each addition

upto a ratio of 1.5:1 metal:ligand. At this point the aliquot size was increased to 50 μL (0.5 equivalents) to a final ratio of 3:1 metal:ligand.

Solution preparation for luminescence studies of Ln^{3+} (Ln = Pr, Tb, Eu) complexation with $CyMe_4$-BTPhen and $CyMe_4$-BTBP. A solution of $CyMe_4$-BTPhen/$CyMe_4$-BTBP in MeOH (120 μL, 1×10^{-4} M) was added to a 1.2 mL quartz cuvette followed by addition of a solution of the $Ln(NO_3)_3$ in MeOH (20 μL, 3×10^{-4} M). The solution was diluted to ~1 mL with MeOH and spectra were obtained.

Solution samples in d_4-methanol were prepared in the same manner as for the MeOH samples but using a 6×10^{-4} M solution of $CyMe_4$-BTPhen/$CyMe_4$-BTBP (20 μL) in d_4-methanol and solutions were diluted using d_4-methanol.

Extracted sample preparation for XAS measurements. Pre-distilled cyclohexanone and a 30 % (v/v) solution of TBP in cyclohexanone were 'washed' before use according to a previously outlined procedures.[27] The washing took place four days before it was used for lanthanide extractions. The extractants $CyMe_4$-BTBP and $CyMe_4$-BTPhen were dissolved in either organic solutions by gentle warming and sonication to a final extractant concentration of 50 mM. Aqueous stock solutions of $Ln(NO_3)_3$ (Ln = Pr, Eu, Tb; 10 mM) were prepared by dissolution of the relevant salt in 4 M HNO_3 in de-ionised H_2O for extractions with 30 % TBP/cyclohexanone, while an aqueous mixture of 1 M HNO_3 and 3 M $NaNO_3$ in de-ionised water was used for extractions with pure cyclohexanone, due to previously reported miscibility issues.[10]

The extractions were performed using 1.0 mL of each phase (organic and aqueous) contained in a 2.5 mL sample vial. The phases were mixed using a Labinco L46 shaker for 5 min. each. Once contacted, each sample had the (lower) aqueous layer syringed out of the vial and

then the (upper) organic layer pipetted into another vial for storage before XAS measurements were performed.

Solid sample preparation for XAS measurements. Solid samples of **2**, **3** and **4** were prepared for XAS measurements by crushing ~ 5-6 mg of the crystalline material in a mortar and pestle, and mixed thouroughly with ~ 90 mg of BN. The homogeneous material was then pressed into flat disks (~ 2 cm diameter).

X-ray crystallography

Diffraction data for $Pr(CyMe_4\text{-}BTPhen)_2(NO_3)](NO_3)_2.10H_2O$ (**1.**$10H_2O$), $[Pr(CyMe_4\text{-}BTPhen)_2(NO_3)][Pr(NO_3)_5].MeOH$ (**2**.MeOH), $[Eu(CyMe_4\text{-}BTPhen)_2(H_2O)](NO_3)_3.9H_2O$ (**3.**$9H_2O$), **[**$Tb(CyMe_4\text{-}BTPhen)_2(H_2O)](NO_3)_3.9H_2O$ (**4**.$9H_2O$), $[Yb(CyMe_4\text{-}BTPhen)_2(H_2O)](NO_3)_3.9H_2O$ (**5**.$9H_2O$), $[Pr(CyMe_4\text{-}BTBP)_2(NO_3)](NO_3)_2.4MeOH.H_2O$ (**6**.$4MeOH.H_2O$) $[Pr(CyMe_4\text{-}BTBP)_2(NO_3)]_2[Pr(NO_3)_6](NO_3).6CH_3CN$ (**7**.$6CH_3CN$), $[Eu(CyMe_4\text{-}BTBP)_2(NO_3)](NO_3)_2.4EtOH.2H_2O$ (**8**.$4EtOH.2H_2O$), $[Eu(CyMe_4\text{-}BTBP)(NO_3)_3]$.toluene (**9**.toluene) and $[Tb(CyMe_4\text{-}BTBP)_2(H_2O)](NO_3)_2.4EtOH$ (**10**.4EtOH) were measured at 100 K with either a Bruker APEX SMART platform CCD area MoKα diffractometer (**2**, **3** and **9**), an Oxford Diffraction XCalibur2 MoKα diffractometer (**1**, **4**, **5**, **6**, **7** and **8**) or a Bruker APEX2 CuKα diffractometer (**10**). All were equipped with a low-temperature device an collections performed at 100 K. CryAlisPro was used to guide the Oxford diffractometer for the collection of a full set of diffraction images and perform unit cell determination and data reduction. These data were corrected for Lorenz and polarization factors, and analytical, multi-scan, absorption corrections applied. BRUKER SMART (MoKα) or

APEX2 (CuKα) was used to guide the Bruker diffractometers and perform unit cell determinations.[28] Reduction of the Bruker collected data was performed using SAINT PLUS (MoKα) or APEX2 (CuKα) and a multiscan absorption correction was performed using SADABS.[29,30] For all crystal data, the structures were solved by direct methods using SIR92.[31] Structure refinement was achieved *via* full matrix least squares based on F^2 using SHELXL97.[32] All non-hydrogen atoms not exhibiting disorder were refined anisotropically, while hydrogen atoms were included in calculated positions. Molecular graphics were generated using ORTEP and all displayed plots show probability ellipsoids of 50 %.[33] In the case of structure **10** modelling of residual solvent molecules was not possible. As such the SQUEEZE procedure in PLATON was used to obtain solvent-free reflection data and subsequent refinement was performed on these data. Where disorder has been modelled over multiple sites this was done using the PART command and is detailed in the relevant CIF (crystallographic information) files (see Supporting information).

General X-ray Absorption Spectroscopy Measurements

Lanthanide (Eu, Tb) L_{III}-edge X-ray absorption spectroscopy (XAS) of extracted solutions and crystalline solids were recorded in transmission and fluorescence modes on beamline B18 at the Diamond Light Source operating in a 10 minute top-up mode for a ring current of 300 mA and an energy of 3 GeV. The radiation was monochromated with a Si(111) double crystal, and harmonic rejection was achieved through the use of two Pt-coated mirrors operating at an incidence angle of 8.3 mrad. The monochromator was calibrated using the K-edge of a Fe foil, taking the first inflexion point in the Fe edge as 7112 eV. Spectra obtained in fluorescence mode utilised a nine element Ge detector. The spectra were summed and background subtracted using the software

package Athena.[34] The spectra were simulated using the software package Artemis which utilises the Feff database in its simulations.[34,35]

Conclusions

The successful characterisation of a series of directly synthesized lanthanide(III) complexes of the tetra-N donor extractants, $CyMe_4$-BTPhen and $CyMe_4$-BTBP, using X-ray diffraction for solid state studies and solution electronic spectroscopy has provided robust chemical models which were used to assist in the determination of lanthanide species formed under proposed conditions for the partitioning of spent nuclear fuel. Simulations of the EXAFS region from X-ray absorption spectra showed the dominant species extracted into the organic phase were dicationic complex species where two N_4-donor extractant ligands and a nitrate ion were coordinated to the Ln^{3+} centre, as mainly observed in the direct synthesis studies. The presence of TBP in the organic phase, which may be used in a potential GANEX separation, clearly showed no influence with regards to lanthanide speciation. Further work will assess the source of the high separation factors these N-donor ligands exhibit for minor actinide/lanthanide partitioning. Similar speciation studies for extracted Am^{3+} and Cm^{3+} in the bulk organic phase will be performed to determine if analogous minor actinide complexes to those observed in the lanthanide studies are formed, or whether separation is achieved by the formation of minor actinide species that are substantially different (e.g. charge neutral tris(nitrate) complex molecules) to those of the lanthanides. Such studies have been performed for BTP (2,6-bis(1,2,4-triazin-3-yl)pyridine) derived extractants and indicate little difference between Eu^{3+} and Cm^{3+} speciation,[36] but this needs to be confirmed for the N_4-donor extractants particularly with respect to the role of nitrate ions in minor actinide/lanthanide coordination. Studies investigating metal speciation at the interfacial region in these liquid-liquid separations will also be conducted to

assess the mechanism by which the minor actinides preferentially cross from the aqueous phase into the organic phase using these organic soluble N-donor extractants, and whether actinide/lanthanide speciation in the bulk organic phase is different to that at the liquid-liquid interface. Understanding the molecular scale processes that underpin techniques for the partitioning of spent nuclear fuel will provide improved development of advanced separation methodologies like SANEX and GANEX.

Acknowledgement. This work is funded by the RCUK Energy Programme through its support of the MBASE consortium. The studentship for DMW was provided by the EPSRC funded Nuclear FiRST Doctoral Training Centre. We thank Diamond Light Source for access to beamline B18 (SP7226) that contributed to the results presented here. We wish to acknowledge the use of the EPSRC funded Chemical Database Service at Daresbury. We also thank Dr John Charnock for his assistance with EXAFS simulations.

Supporting Information Available. Plots of single crystal XRD structures, crystallographic information files (CIF), UV-visible absorption, excitation and emission spectra, and X-ray absorption spectra with corresponding fits and parameters for the EXAFS data region.

Corresponding Author

*Email: clint.a.sharrad@manchester.ac.uk. Tel:+44 161 275 4657. Fax: +44 161 306 9321.

FIGURE CAPTIONS

Figure 1. Structural diagrams for $CyMe_4$-BTBP (*left*) and $CyMe_4$-BTPhen (*right*).

Figure 2. UV-visible absorption spectroscopic titration of $CyMe_4$-BTPhen with $Pr(NO_3)_3$ in methanol.

Figure. 3. UV-visible absorption spectroscopic titration of $CyMe_4$-BTBP with $Eu(NO_3)_3$ in methanol.

Figure 4. Emission (following excitation at 320 nm), excitation (monitoring emission at 616 nm) and absorption spectra of $[Eu(CyMe_4\text{-}BTPhen)_2(X)]^{n+}$ in methanol ($X = H_2O/NO_3^-$; n = 3,2).

Figure 5. Time resolved emission spectrum of $[Eu(CyMe_4\text{-}BTPhen)_2(X)]^{n+}$ in methanol following excitation at 320 nm ($X = H_2O/NO_3^-$; n = 3,2).

Figure 6. ORTEP plot of the complex cation of **1**, with crystallographic numbering (hydrogens omitted).

Figure 7. ORTEP plot of the complex cation of **3**, with crystallographic numbering (hydrogens omitted).

Figure 8. ORTEP plot of the complex cation of **8**, with crystallographic numbering (hydrogens omitted).

Figure 9. ORTEP plot of the complex molecule of **9**, with crystallographic numbering (hydrogens omitted).

Figure 10. ORTEP plot of the complex cation of **10**, with crystallographic numbering (hydrogens omitted).

Figure 11. Eu L_{III}-edge X-ray absorption spectra of $CyMe_4$-BTPhen containing species.

Figure 12. Tb L_{III}-edge X-ray absorption spectra of $CyMe_4$-BTPhen containing species.

Figure 13. Eu L_{III}-edge EXAFS spectrum (Fourier transform in R space) of the extraction of $Eu(NO_3)_3$ with $CyMe_4$-BTPhen in cyclohexanone, fitted to $[Eu(CyMe_4\text{-}BTBP)_2(NO_3)]^{2+}$ (*upper* plot generated from the real part of $\chi(R)$, *lower* plot generated from the imaginary part of $\chi(R)$).

REFERENCES

1 O'Boyle, N. C.; Nicholson, G. P.; Piper, T. J.; Taylor, D. M.; Williams, D. R.; Williams, G. *Appl. Radiat. Isotopes* **1997**, *48*, 183-200.

2 Sessler, J. L.; Melfi, P. J.; Pantos, G. D. *Coordin. Chem. Rev.* **2006**, *250*, 816-843.

3 Madic, C.; Boullis, B.; Baron, P.; Testard, F.; Hudson, M. J.; Liljenzin, J. -O.; Christiansen, B.; Ferrando, M.; Facchini, A.; Geist, A.; Modolo, G.; Espartero, A. G.; De Mendoza, J. *J. Alloy Compd.* **2007**, *444-445*, 23-27.

4 (a) Alstad, J.; Jahnsen, T.; Pappas, A. C. *J. Inorg. Nucl. Chem.* **1967**, *29*, 2155-2160. (b) Caldwell, J. T.; Dowdy, E. J.; Berman, B. L.; Alvarez, R. A.; Meyer, P. *Phys. Rev. C* **1980**, *21*, 1215-1231.

5 *The Nuclear Fuel Cycle*; Wilson, P. D., Ed.; Oxford University Press: Oxford, 1986.

6 Modolo, G.; Vijgen, H.; Serrano-Purroy, D.; Christiansen, B.; Malmbeck, R.; Baron, P. *Sep. Sci. Technol.* **2007**, *42*, 439.

7 Vandegrift, G. F.; Chamberlain, D. B.; Connor, C.; Copple, J. M.; Dow, J. A.; Everson, L.; Hutter, J. C.; Leonard, R. A.; Nunez, L.; Regalbuto, M. C.; Sedlet, J.; Srinivasen, B.; Weber, S.; Wygmans, D. G. *Proceedings of the Symposium on Waste Management*, Arizona, USA, 1993.

8 Magnusson, D.; Christiansen, B.; Foreman, M. R. S.; Geist, A.; Glatz, J. -P.; Malmbeck, R.; Modolo, G.; Serrano-Purroy, D.; Sorel, C. *Solvent Extr. Ion Exc.* **2009**, *27*, 97-106.

9 Lewis, F. W.; Harwood, L. M.; Hudson, M. J.; Drew, M. G. B.; Desreux, J. F.; Vidick, G.; Bouslimani, N.; Modolo, G.; Wilden, A.; Sypula, M.; Vu, T.-H.; Simonin, J.-P. *J. Am. Chem. Soc.* **2011**, *133*, 13093–13102.

10 Aneheim, E.; Ekberg, C.; Fermvik, A.; Foreman, M. R. St. J.; Retegan, T.; Skarnemark, G. *Solvent Extr. Ion Exch.* **2010**, *28*, 437-458.

11 Foreman, M. R. S.; Hudson, M. J.; Drew, M. G. B.; Hill, C.; Madic, C. *Dalton Trans.* **2006**, 1645-1653.

12 Lewis, F. W.; Harwood, L. M.; Hudson, M. J.; Drew, M. G. B.; Sypula, M.; Modolo, G.; Whittaker, D.; Sharrad, C. A.; Videva, V.; Hubscher-Bruder, V.; Arnaud-Neu, F. *Dalton Trans.* **2012**, *41*, 9209-9219.

13 Natrajan, L. S.; Khoabane, N. M.; Dadds, B. L.; Muryn, C. A.; Pritchard, R. G.; Heath, S. L.; Kenwright, A. M.; Kuprov, I.; Faulkner, S. *Inorg. Chem.* **2010**, *49*, 7700-7709.

14 (a) Richardson, F. S. *Chem. Rev.* **1982**, *82*, 541-552. (b) Natrajan, L S.;.Blake, A. J.; Wilson, C; Weinstein, J. A.; Arnold, P. L. *Dalton Trans*. **2004**, 3748-3755.

15 Tedeshi, C.; Picaud, C.; Azéma, J.; Donnadieu, B.; Tisnès, P. *New J. Chem.* **2000**, *24*, 735-737.

16 (a) Beeby, A.; Clarkson, I. M.; Dickins, R. S.; Faulkner, S.; Parker, D.; Royle, L.; de Sousa, A. S.; Williams, J. A. G.; Woods, M. *J. Chem. Soc*., *Perkin Trans. 2*, **1999**, 493–503. (b) Zhao, Y.-F.; Zhao, Y.-L.; Bai, F.; Wei, X.-Y.; Zhou, Y.-S.; Shan, M.-Na; Li, H.-H.; Ma, R.-J.; Fu, X.-T; Du, Y. *J. Fluoresc.* **2010**, *20*, 763–770.

17 (a) Fletcher, D. A.; McMeeking, R. F.; Parkin, D. *J. Chem. Inf. Comput. Sci.* **1996**, *36*, 746-749. (b) Allen, F. H. *Acta Crystallogr.*, **2002**, *B58*, 380-388. (c) Bruno, I. J.; Cole, J. C.; Edgington, P. R.; Kessler, M.; Macrae, C. F.; McCabe, P.; Pearson, J.; Taylor, R. *Acta Crystallogr*. **2002**, *B58*, 389-397. (d) Macrae, C. F.; Edgington, P. R.; McCabe, P.; Pidcock, E.; Shields, G. P.; Taylor, R.; Towler, M.; van de Streek, J. *J. Appl. Cryst.* **2006**, *39*, 453-457.

18 (a) Cotton, S. A.; Franckevicius, V.; Mahon, M. F.; Ling Ooi; L.; Raithby, P. R.; Teat, S. J. *Polyhedron* **2006**, *25*, 1057-1068. (b) Kaczmarek, A. M.; Kubicki, M.; Pospieszna-

Markiewicz, I.; Radecka-Paryzek, W. *Inorg. Chim. Acta* **2011**, *365*, 137-142. (c) Merkel, M.; Pascaly, M.; Köster, C.; Krebs, B. *Z. Naturforsch B* **2004**, *59*, 216-220

19 Steppert, M.; Cisařová, I.; Fanghänel, T.; Geist, A.; Lindqvist-Reis, P.; Panak, P.; Štěpnička, P.; Trumm, S.; Walther, C. *Inorg. Chem.* **2012**, *51*, 591-600.

20 Berthet, J. -C.; Thuéry, P.; Foreman, M. R. S.; Ephritikhine, M. *Radiochim. Acta* **2008**, *96*, 189-197.

21 (a) Gregloński, G.; Lisowski, L. *Angew. Chem. Int. Ed.* **2006**, *45*, 6122-6126. (b) Visinescu, D.; Fabelo, O.; Ruiz-Pérez, C.; Lloret, F.; Julve, M. *CrystEngComm* **2010**, *12*, 2454-2465.

22 Lam, A. W.-H.; Wong, W.-T.; Wen, G.; Zhang, X-X.; Gao, S. *New J. Chem.* **2001**, *25*, 531-533.

23 (a) Guo, Y.; Dou, W.; Zhou, X.; Liu, W.; Qin, W.; Zang, Z.; Zhang, H.; Wang, D. *Inorg. Chem.* **2009**, *48*, 3581-3590 (b) Wałęsa-Chorab, M.; Gorczyński, A.; Kubicki, M.; Hnatejko, Z.; Patroniak, V. *Polyhedron* **2012**, *31*, 51-57.

24 The C shell closest to the Ln centre is comprised of the carbon atoms from the N_4-donor ligands that are immediately adjacent to the coordinating N atoms.

25 The outer C shells are comprised of the carbon atoms from the N_4-donor ligands that are located at the *meta* and *para* positions relative to the coordinating N atoms.

26 (a) Feng, M.-L.; Mao, J.-G. *Eur. J. Inorg. Chem.* **2007**, *34*, 5447-5454. (b) Zhou, X.-H.; Peng, Y.-H.; Du, X.-D.; Wang, C.-F.; Zuo, J.-L; You, X.-Z. *Cryst. Growth Des.* **2009**, *9*, 1028-1035. (c) Zhang, Z.-J.; Shi, W.; Huang, Y.-Q.; Zhao, B.; Cheng, P.; Liao, D.-Z.; Yan. S.-P. *CrystEngComm* **2009**, *11*, 1811-1814.

27 Sarsfield, M. J.; Taylor, R. J.; Maher, C. J. *Radiochim. Acta* **2007**, *95*, 677–682.

28 Bruker (2001), SMART, Version 5.625, Bruker AXS Inc., Madison, Wisconsin, USA.

29 Bruker (2002), SAINT, Version 6.36a, Bruker AXS Inc., Madison, Wisconsin, USA.

30 Bruker (2001), SADABS, Version 2.03a, Bruker AXS Inc., Madison, Wisconsin, USA.

31 Altomare, A.; Cascarano, G.; Giacovazzo, C.; Guagliardi, A. *J. Appl. Crystallogr.* **1993**, *26*, 343-350.

32 Sheldrick, G. M. *SHELXL97, Programs for Crystal Structure Analysis (Release 97-2)*, University of Göttingen, Germany, 1998.

33 Farrugia, L. J. *J. Appl. Crystallogr.* **1997**, *30*, 565.

34 Ravel B.; Newville, M. *J. Synchrotron Rad.* **2005**, *12*, 537-541.

35 Newville, M. *J. Synchrotron Rad.* **2001**, *8*, 322-324.

36 Denecke, M. A.; Rossberg, A.; Panak, P. J.; Weigl, M.; Schimmelpfennig, B.; Geist, A. *Inorg. Chem.* **2005**, *44*, 8418-8425.

Tables

Table 1. Photophysical properties of solutions of $Ln(NO_3)_3$ with tetra-N donor ligands in a 1:2 molar ratio at 298 K*

Complex	λ_{em} (nm)	τ_{MeOH} (ms)	τ_{MeOD} (ms)	q_{MeOH}
$[Eu(BTBP)_2(X)]^{n+}$	617	1.94	2.61	0.3
$[Eu(BTPhen)_2(X)]^{n+}$	617	1.49	1.87	0.3

*All lifetimes recorded by TCSPC at 320 nm excitation using a 5W Xenon flashlamp and are subject to a ± 10 % error. Identical data within error were obtained for 1:3 and 1:5 solutions of Eu^{3+}:$L_{N4\text{-}donor}$, and the crystalline complexes **3** and **8**.

Table 2. Crystal data for complexes **1-5**

	[Pr(CyMe$_4$-BTPhen)$_2$(NO$_3$)](NO$_3$)$_2$.10H$_2$O **1**	**[Pr(CyMe$_4$-BTPhen)$_2$(NO$_3$)][Pr(NO$_3$)$_5$].1.63EtOH.0.37H$_2$O** **2**	**[Eu(CyMe$_4$-BTPhen)$_2$(H$_2$O)](NO$_3$)$_3$.9H$_2$O** **3**	**[Tb(CyMe$_4$-BTPhen)$_2$(H$_2$O)](NO$_3$)$_3$.9H$_2$O** **4**	**[Yb(CyMe$_4$-BTPhen)$_2$(H$_2$O)](NO$_3$)$_3$.9H$_2$O** **5**
Formula	$C_{68}H_{96}N_{19}O_{19}Pr$	$C_{71.25}H_{87.25}N_{22}O_{20.38}Pr_2$	$C_{68}H_{96}N_{19}O_{19}Eu$	$C_{68}H_{96}N_{19}O_{19}Tb$	$C_{68}H_{96}N_{19}O_{19}Yb$
M	1624.39	1859.70	1615.44	1642.56	1656.68
Crystal System	Monoclinic	Triclinic	Orthorhombic	Orthorhombic	Orthorhombic
a (Å)	31.654(5)	13.716(5)	31.172(3)	31.3486(7)	31.3257(13)
b (Å)	26.271(5)	15.221(5)	38.128(3)	38.0261(9)	37.709(2)
c (Å)	19.501(5)	20.359(5)	14.8296(13)	14.8414(3)	14.8783(7)
α (°)	90	107.225(5)	90	90	90
β (°)	109.504(5)	99.422(5)	90	90	90
γ (°)	90	97.083(5)	90	90	90
Space Gp.	C2/c	P-1	Fdd2	Fdd2	Fdd2
Z	8	2	8	8	8
T (K)	100(2)	100(2)	100(2)	100(2)	100(2)
μ (mm^{-1})	0.718	1.309	0.782	0.867	1.135
Reflns. Measd	20981	25422	32709	49820	8497
Reflns. Obsd	6002	14178	8290	9044	5110
R_1 (obsd)	0.0551	0.0547	0.0512	0.0513	0.0658
wR^2(all data)	0.1271	0.1393	0.1364	0.1423	0.1984

Table 3. Crystal data for complexes **6 - 10**

	$[Pr(CyMe_4\text{-}BTBP)_2(NO_3)](NO_3)_2.4MeOH.H_2O$ **6**	**$[Pr(CyMe_4\text{-}BTBP)_2(NO_3)]_2[Pr(NO_3)_6](NO_3).6CH_3CN$** **7**	**$[Eu(CyMe_4\text{-}BTBP)_2(NO_3)](NO_3)_2.4EtOH.2H_2O$** **8**	**$[Eu(CyMe_4\text{-}BTBP)(NO_3)_3].toluene$** **9**	**$[Tb(CyMe_4\text{-}BTBP)_2(H_2O)](NO_3)_3.4EtOH$** **10**
Formula	$C_{72}H_{102}N_{19}O_{14}Pr$	$C_{140}H_{166}N_{47}O_{27}Pr_3$	$C_{72}H_{104}N_{19}O_{15}Eu$	$C_{46}H_{54}N_{11}O_9Eu$	$C_{72}H_{102}N_{19}O_{14}Tb$
M	1598.64	3361.93	1627.68	1056.96	1614.63
Crystal System	Monoclinic	Monoclinic	Orthorhombic	Monoclinic	Monoclinic
a (Å)	24.2790(7)	16.604(2)	16.4128(6)	26.385(2)	30.5621(7)
b (Å)	16.5467(4)	28.1161(19)	23.8916(6)	11.6674(11)	14.8217(4)
c (Å)	19.4601(5)	17.7385(14)	19.7838(6)	15.7469(14)	23.9083(6)
α (°)	90	90	90	90	90
β (°)	90.355(3)	106.609(10)	90	90.6730(10)	129.4280(10)
γ (°)	90	90	90	90	90
Space Gp.	$P2_1/c$	$P2_1/n$	Pccn	C2/c	C2/c
Z	4	2	4	4	4
T (K)	100(2)	100(2)	100(2)	100(2)	100(2)
μ (mm^{-1})	0.697	0.988	0.884	1.359	4.723
Reflns. Measd	77969	17453	47979	17887	25718
Reflns. Obsd	13767	17454	6854	4618	7271
R_1 (obsd)	0.0562	0.0766	0.1158	0.0430	0.0919
wR^2(all data)	0.1435	0.2209	0.2628	0.1164	0.2387

Table 4. Selected interatomic distances (Å) for $CyMe_4$-BTPhen containing complexes **1-5**

Bond	**Origin**	**1 (Pr)**	**2 (Pr)**	**3 (Eu)**	**4 (Tb)**	**5 (Yb)**
N2-M	$N_{triazinyl}$	2.637(9)	2.645(6)	2.539(5)	2.527(5)	2.475(8)
N6-M		2.62(1)	2.634(6)	2.541(6)	2.516(6)	2.51(1)
N10-M		2.623(8)	2.567(7)	N/A	N/A	N/A
N14-M		2.618(9)	2.591(6)	N/A	N/A	N/A
N4-M	N_{phen}	2.669(8)	2.633(6)	2.507(5)	2.485(4)	2.42(1)
N5-M		2.637(9)	2.587(6)	2.523(5)	2.499(5)	2.44(1)
N12-M		2.675(8)	2.617(6)	N/A	N/A	N/A
N13-M		2.638(8)	2.583(7)	N/A	N/A	N/A
O1-M	O_{Water}	N/A	N/A	2.414(6)	2.397(6)	2.37(1)
O1-M	$O_{Nitrate}$	2.592(8)	2.581(4)	N/A	N/A	N/A
O2-M		2.542(8)	2.604(5)	N/A	N/A	N/A

Table 5. Selected interatomic distances (Å) for $CyMe_4$-BTBP containing complexes **6**-**10**

Bond	Origin	6 (Pr)	7 (Pr)	8 (Eu)	9 (Eu)	10 (Tb)
N2-M	$N_{triazinyl}$	2.637(5)	2.654(9)	2.566(9)	2.532(4)	2.516(6)
N6-M		2.597(6)	2.595(9)	2.58(1)	N/A	2.512(5)
N10-M		2.611(5)	2.580(8)	N/A	N/A	N/A
N14-M		2.634(5)	2.60(1)	N/A	N/A	N/A
N4-M	N_{bipy}	2.639(5)	2.65(1)	2.57(1)	2.544(4)	2.487(5)
N5-M		2.622(5)	2.66(1)	2.562(9)	N/A	2.50(1)
N12-M		2.615(5)	2.649(9)	N/A	N/A	N/A
N13-M		2.632(5)	2.68(1)	N/A	N/A	N/A
O1-M	O_{Water}	N/A	N/A	N/A	N/A	2.407(7)
O1-M	$O_{Nitrate}$	2.596(6)	2.607(8)	2.56(1)	2.548(4)	N/A
O2-M		2.608(6)	2.625(7)	N/A	2.487(3)	N/A
O7-M		N/A	N/A	N/A	2.456(4)	N/A

Table 6. Eu L_{III}-edge EXAFS data[a]

Physical state	Aqueous phase	Organic phase extractants	Chemical composition used in simulation models	Occupancy[b]	Interatomic distances[c] (Å)	σ^2 (Å^2)[d]	r[e]
Solution	$Eu(NO_3)_3$	$CyMe_4$-BTBP	$[Eu(CyMe_4\text{-}BTBP)_2(NO_3)]^{2+}$	Eu-O(2) Eu-N(8) Eu-N(1) Eu-C(10) Eu-C(16) Eu-C(8)	2.38 2.55 3.05 3.45 4.52 4.95	0.022 0.0045 0.00086 0.0031 0.0094 0.0027	0.0108
Solution	$Eu(NO_3)_3$	$CyMe_4$-BTBP + TBP	$[Eu(CyMe_4\text{-}BTBP)_2(NO_3)]^{2+}$	Eu-O(2) Eu-N(8) Eu-N(1) Eu-C(8) Eu-C(16) Eu-C(8)	2.34 2.55 3.03 3.45 4.51 4.95	0.013 0.0043 0.0020 0.00077 0.0098 0.0043	0.0141
Solution	$Eu(NO_3)_3$	$CyMe_4$-BTPhen	$[Eu(CyMe_4\text{-}BTPhen)_2(NO_3)]^{2+}$	Eu-O(2) Eu-N(8) Eu-N(1) Eu-C(8) Eu-C(14) Eu-C(8)	2.43 2.56 3.02 3.46 4.54 4.98	0.0023 0.0054 0.0023 0.00078 0.0073 0.0031	0.0116
Solution	$Eu(NO_3)_3$	$CyMe_4$-BTPhen + TBP	$[Eu(CyMe_4\text{-}BTPhen)_2(NO_3)]^{2+}$	Eu-O(2) Eu-N(8) Eu-N(1) Eu-C(8) Eu-C(14) Eu-C(8)	2.44 2.56 3.01 3.45 4.53 4.98	0.022 0.0054 0.00038 0.00037 0.0068 0.0036	0.0146
Solid	N/A	N/A	$[Eu(CyMe_4\text{-}BTPhen)_2(NO_3)]^{2+}$	Eu-O(2) Eu-N(8) Eu-N(1) Eu-C(8)	2.36 2.54 3.00 3.44	0.024 0.0059 0.00076 0.0022	0.0085

				Eu-C(14)	4.53	0.0092	
				Eu-C(8)	4.96	0.0067	
			$[Eu(CyMe_4\text{-}BTPhen)_2(H_2O)]^{3+}$	Eu-O(1)	2.29	0.012	0.019
				Eu-N(8)	2.54	0.0054	
				Eu-C(8)	3.44	0.0023	
				Eu-C(14)	4.53	0.0089	
				Eu-C(8)	4.96	0.0069	

a S_0^2 is fixed at 1. *b* Occupancy numbers, held constant at given values. *c* ± 0.02 Å. *d* Debye-Waller factors. *e* Parameter describing goodness of fit = weighted sum of squares of residuals divided by the degree of freedom.

Table 7. Tb L_{III}-edge EXAFS data[a]

Physical state	Aqueous phase	Organic phase extractants	Chemical composition used in simulation models	Occupancy[b]	Interatomic Distances (Å)[c]	σ^2 (Å^2)[d]	r[e]
Solution	$Tb(NO_3)_3$	$CyMe_4$-BTBP	$[Tb(CyMe_4\text{-}BTBP)_2(NO_3)]^{2+}$	Tb-O(2) Tb-N(8) Tb-N(1) Tb-C(8) Tb-C(14) Tb-C(8)	2.37 2.51 2.93 3.42 4.47 4.92	0.024 0.0063 0.0028 0.0014 0.0079 0.0017	0.0094
Solution	$Tb(NO_3)_3$	$CyMe_4$-BTBP + TBP	$[Tb(CyMe_4\text{-}BTBP)_2(NO_3)]^{2+}$	Tb-O(2) Tb-N(8) Tb-N(1) Tb-C(8) Tb-C(14) Tb-C(8)	2.34 2.51 2.93 3.41 4.46 4.92	0.013 0.0055 0.0036 0.0017 0.0065 0.0015	0.014
Solution	$Tb(NO_3)_3$	$CyMe_4$-BTPhen	$[Tb(CyMe_4\text{-}BTPhen)_2(NO_3)]^{2+}$	Tb-O(2) Tb-N(8) Tb-N(1) Tb-C(8) Tb-C(14) Tb-C(8)	2.37 2.52 2.93 3.42 4.49 4.94	0.023 0.0062 0.0068 0.0015 0.0072 0.0020	0.012
Solution	$Tb(NO_3)_3$	$CyMe_4$-BTPhen + TBP	$[Tb(CyMe_4\text{-}BTPhen)_2(NO_3)]^{2+}$	Tb-O(2) Tb-N(8) Tb-N(1) Tb-C(8) Tb-C(14) Tb-C(8)	2.39 2.52 2.94 3.42 4.48 4.95	0.022 0.0063 0.0020 0.0011 0.0067 0.0018	0.014
Solid	N/A	N/A	$[Tb(CyMe_4\text{-}BTPhen)_2(NO_3)]^{2+}$	Tb-O(2) Tb-N(8) Tb-N(1) Tb-C(8)	2.32 2.52 2.95 3.42	0.021 0.0064 0.0094 0.0019	0.013

				Tb-C(14)	4.49	0.0098	
				Tb-C(8)	4.93	0.0036	
			$[Tb(CyMe_4\text{-}BTPhen)_2(H_2O)]^{3+}$	Tb-O(1)	2.25	0.011	0.016
				Tb-N(8)	2.51	0.0061	
				Tb-C(8)	3.42	0.0021	
				Tb-C(14)	4.49	0.0097	
				Tb-C(8)	4.93	0.0036	

a S_0^2 is fixed at 1. *b* Occupancy numbers, held constant at given values. *c* ± 0.02 Å. *d* Debye-Waller factors. *e* Parameter describing goodness of fit = weighted sum of squares of residuals divided by the degree of freedom.

Figures

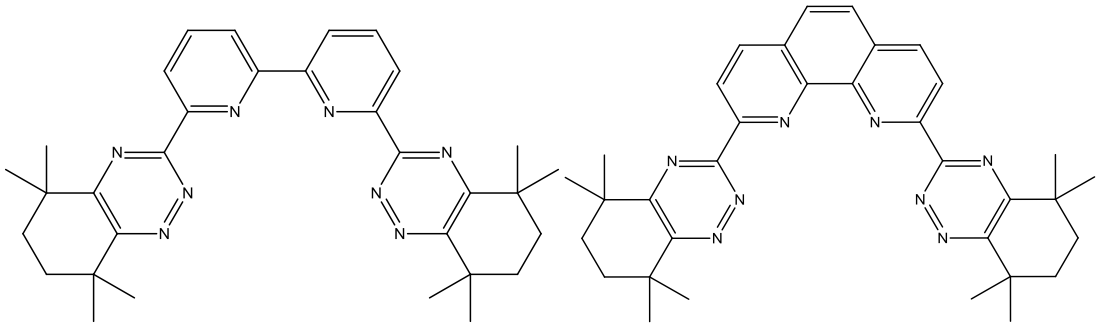

Figure 1. Structural diagrams for $CyMe_4$-BTBP (*left*) and $CyMe_4$-BTPhen (*right*).

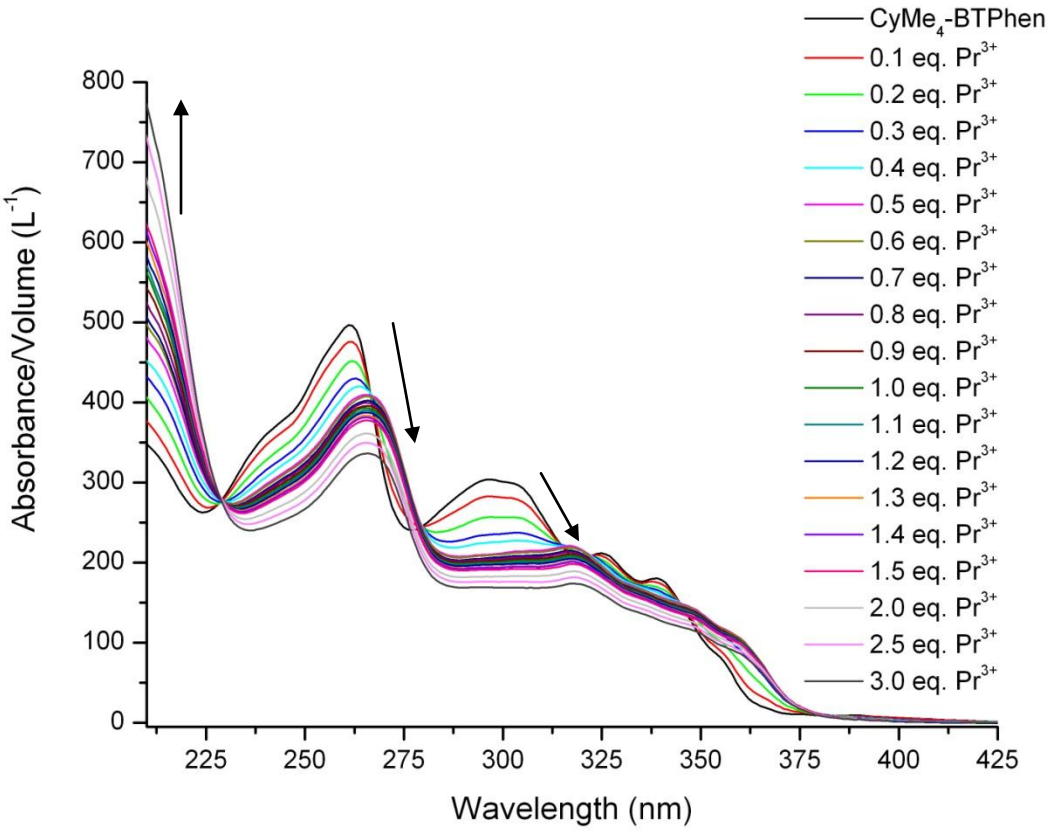

Figure 2. UV-visible absorption spectroscopic titration of $CyMe_4$-BTPhen with $Pr(NO_3)_3$ in methanol.

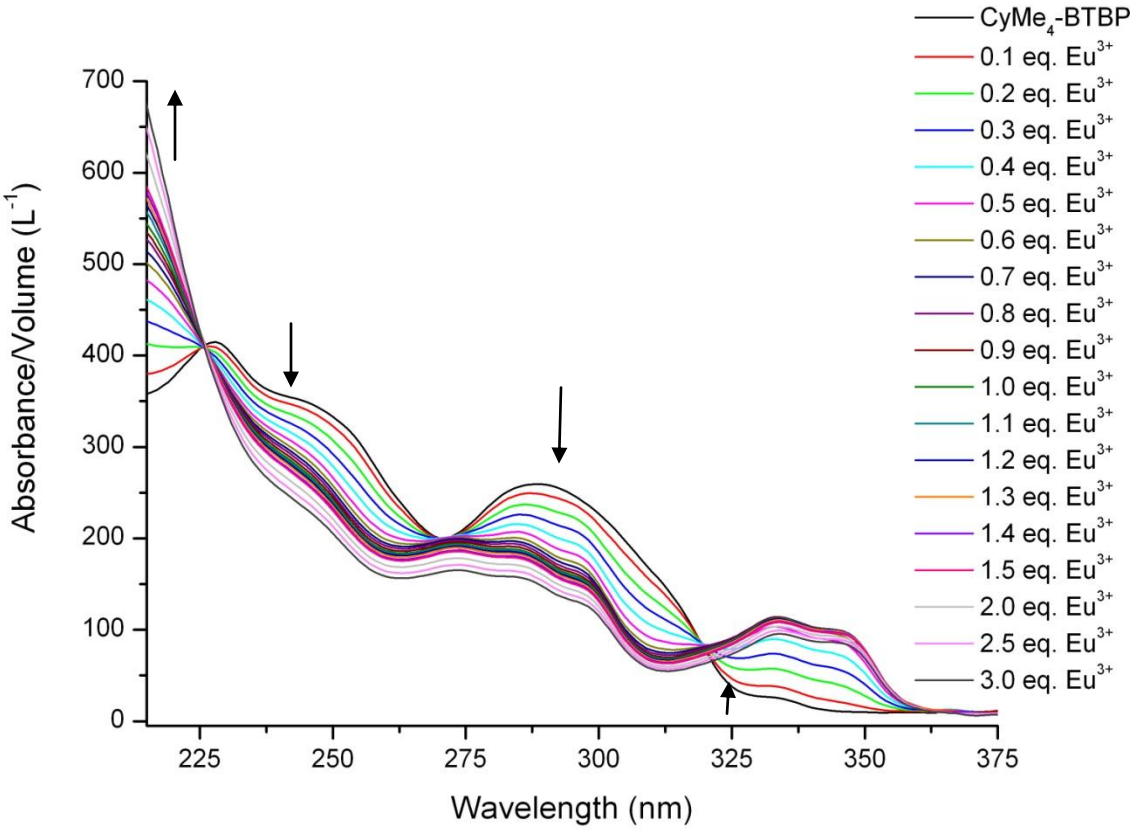

Figure. 3. UV-visible absorption spectroscopic titration of $CyMe_4$-BTBP with $Eu(NO_3)_3$ in methanol.

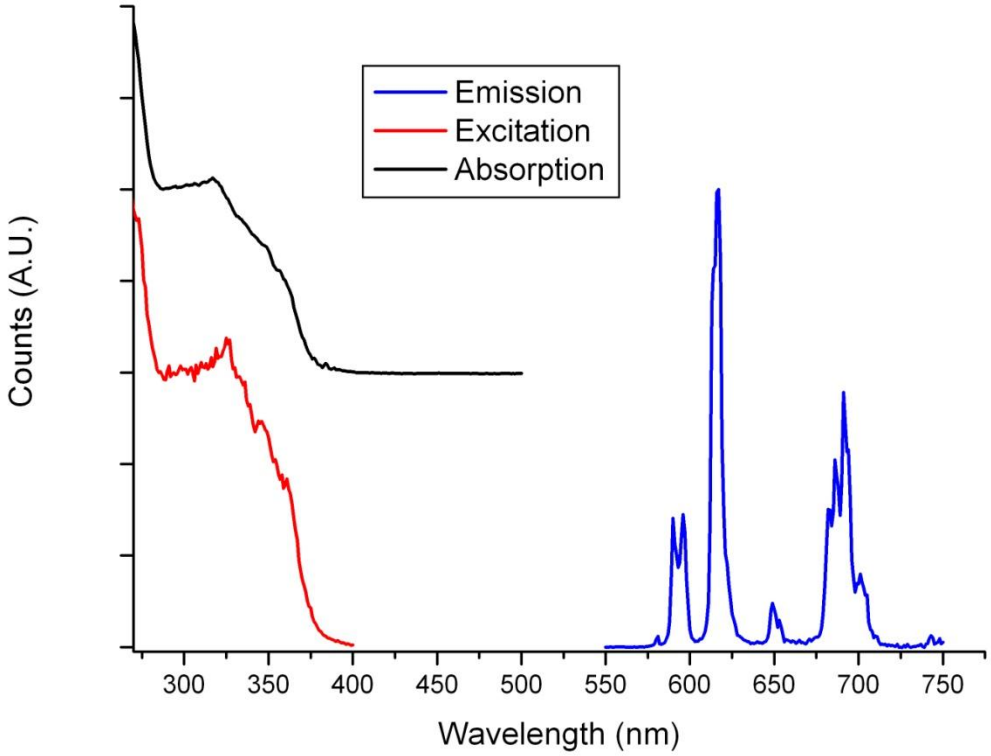

Figure 4. Emission (following excitation at 320 nm), excitation (monitoring emission at 616 nm) and absorption spectra of $[Eu(CyMe_4\text{-}BTPhen)_2(X)]^{n+}$ in methanol ($X = H_2O/NO_3^-$; n = 3,2)

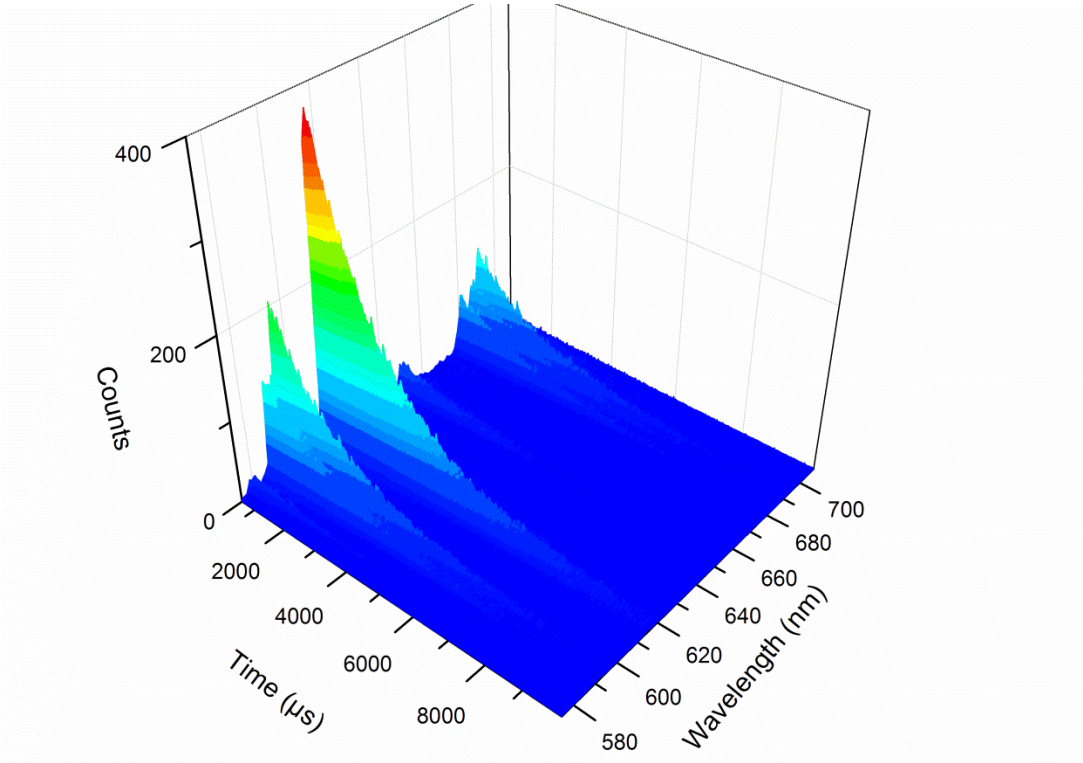

Figure 5. Time resolved emission spectrum of $[Eu(CyMe_4\text{-}BTPhen)_2(X)]^{n+}$ in methanol following excitation at 320 nm ($X = H_2O/NO_3^-$; n = 3,2).

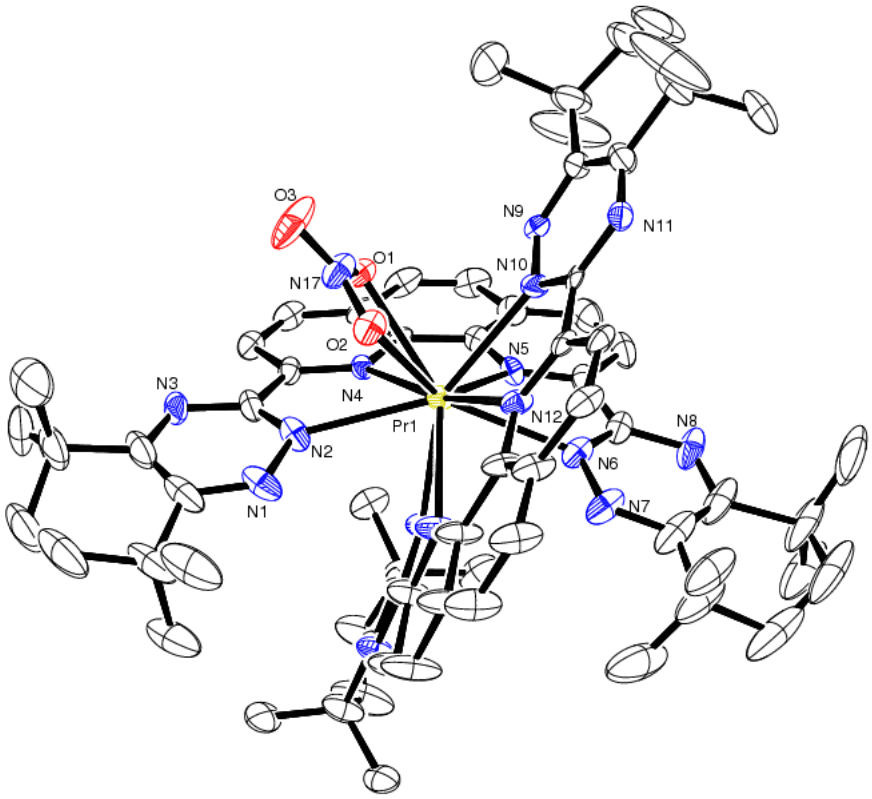

Figure 6. ORTEP plot of the complex cation of **1**, with crystallographic numbering (hydrogens omitted).

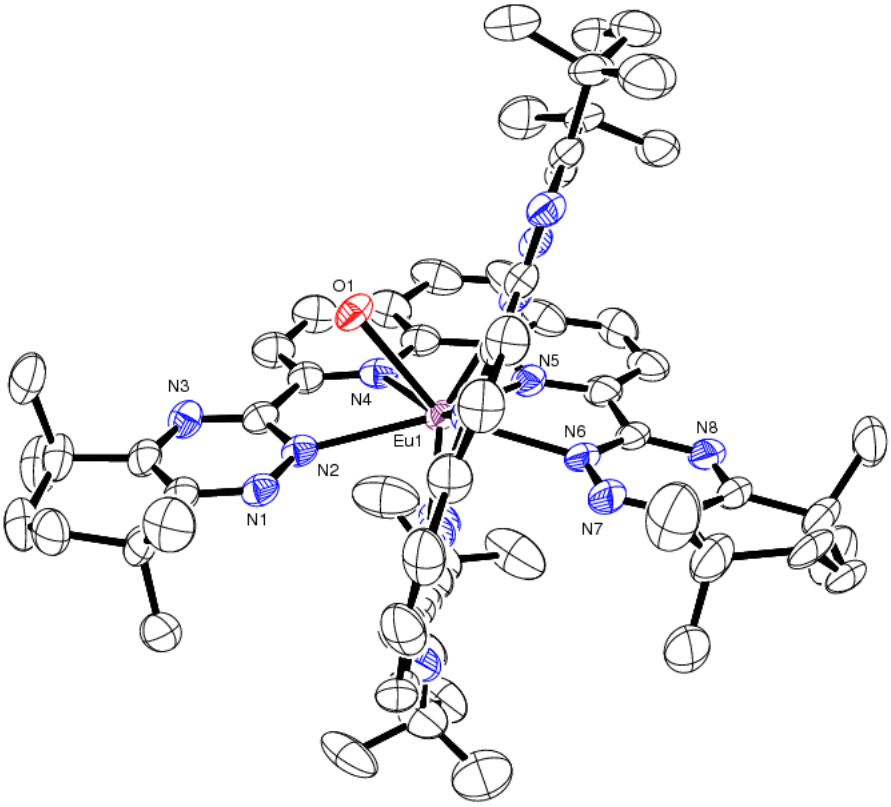

Figure 7. ORTEP plot of the complex cation of **3**, with crystallographic numbering (hydrogens omitted).

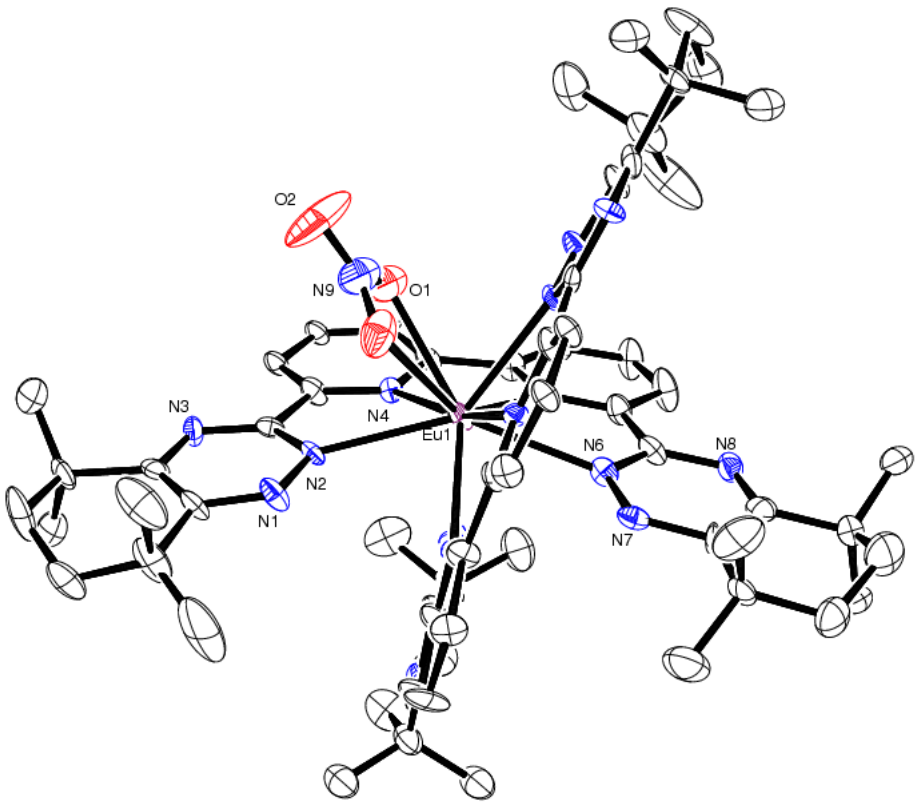

Figure 8. ORTEP plot of the complex cation of **8**, with crystallographic numbering (hydrogens omitted).

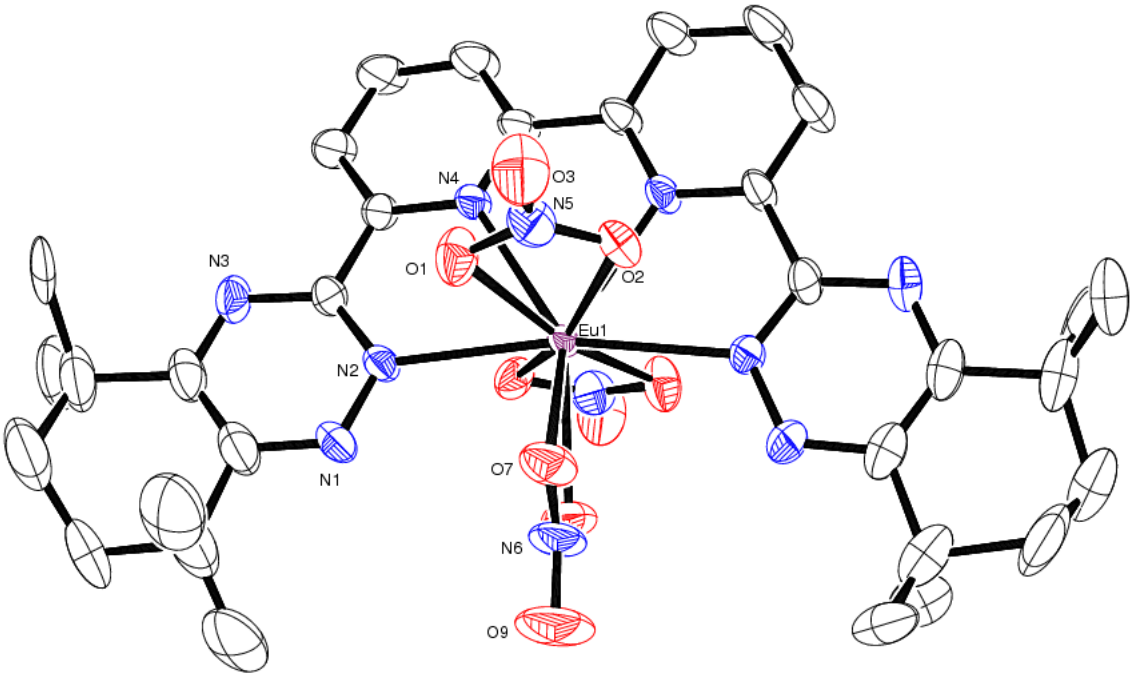

Figure 9. ORTEP plot of the complex molecule of **9**, with crystallographic numbering (hydrogens omitted).

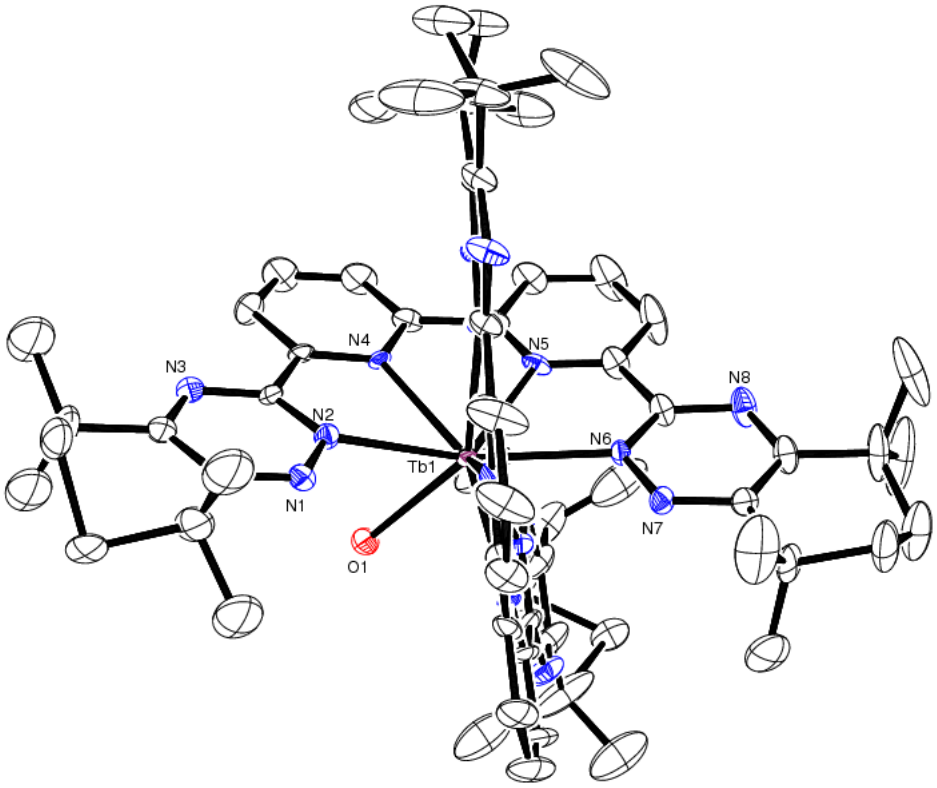

Figure 10. ORTEP plot of the complex cation of **10**, with crystallographic numbering (hydrogens omitted).

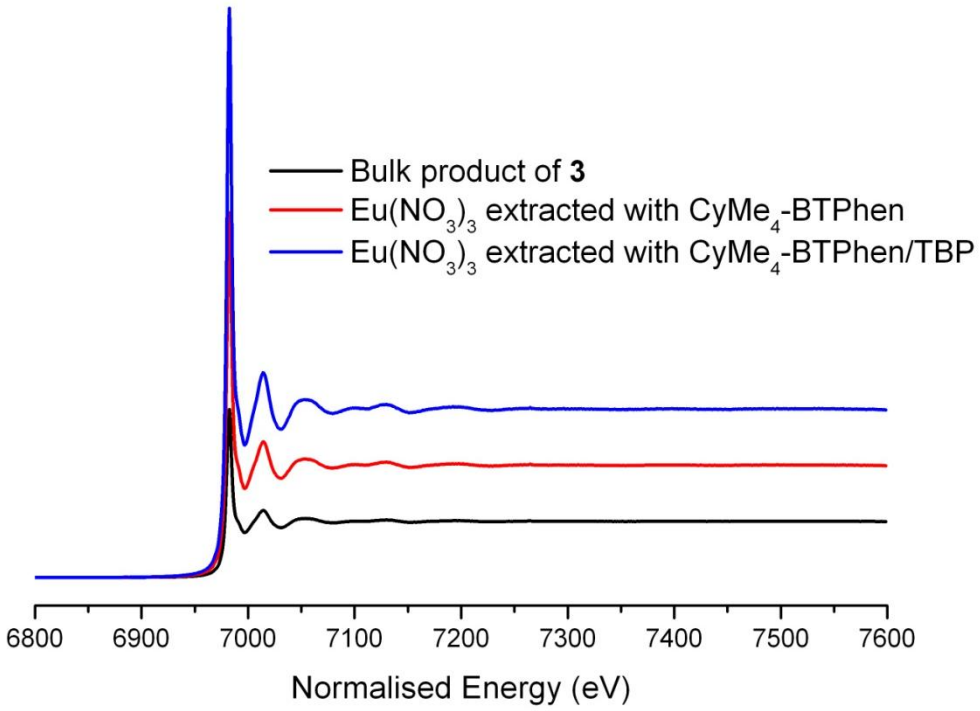

Figure 11. Eu L_{III}-edge X-ray absorption spectra of $CyMe_4$-BTPhen containing species.

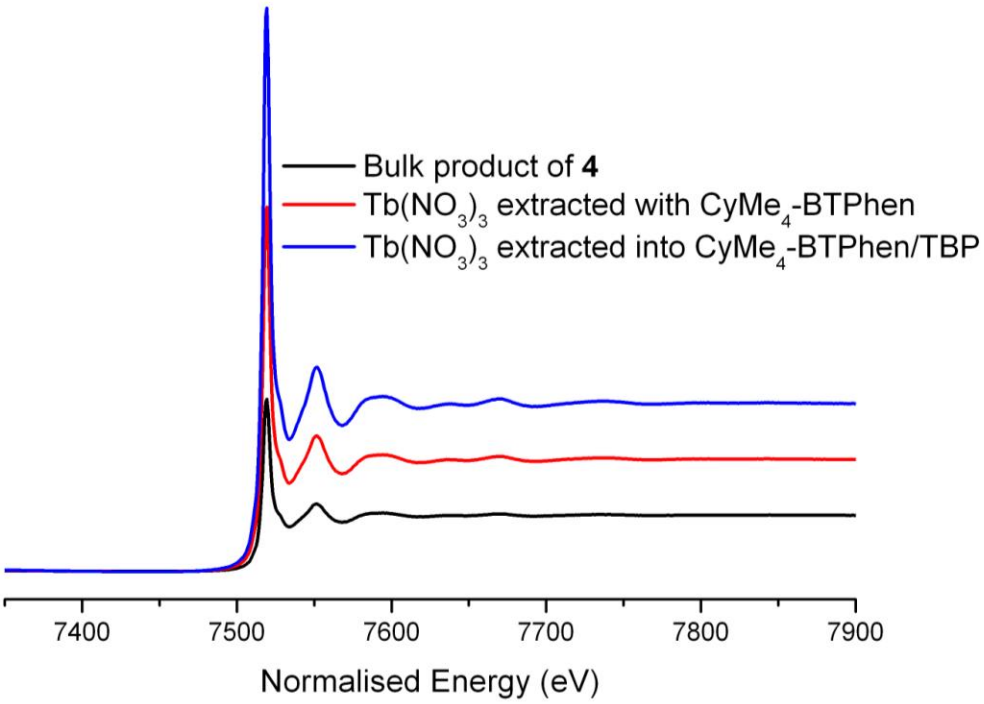

Figure 12. Tb L_{III}-edge X-ray absorption spectra of $CyMe_4$-BTPhen containing species.

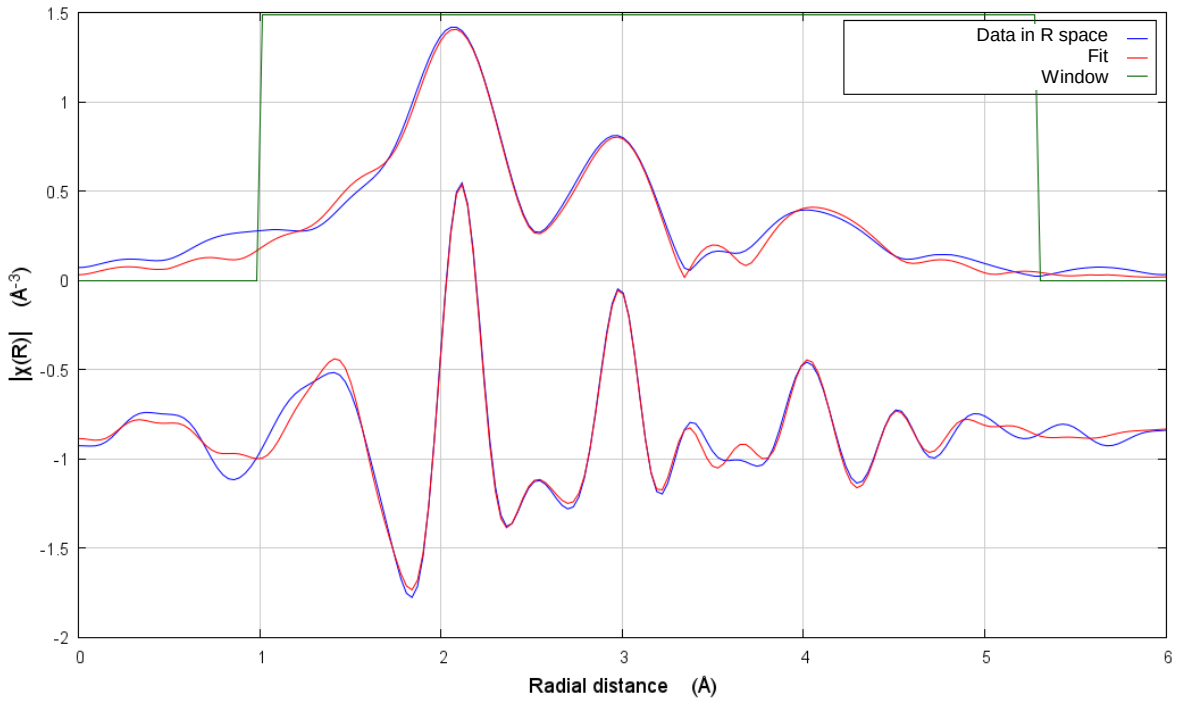

Figure 13. Eu L_{III}-edge EXAFS spectrum (Fourier transform in R space) of the extraction of $Eu(NO_3)_3$ with $CyMe_4$-BTPhen in cyclohexanone, fitted to $[Eu(CyMe_4\text{-}BTBP)_2(NO_3)]^{2+}$ (*upper* plot generated from the real part of $\chi(R)$, *lower* plot generated from the imaginary part of $\chi(R)$).

SYNOPSIS TOC

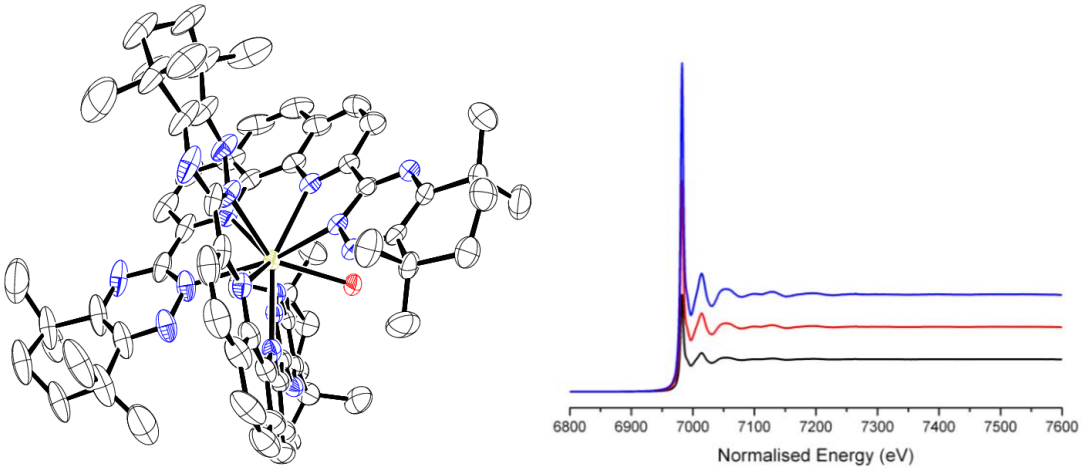

A series of lanthanide(III) complexes with the nitrogen donor extractant molecules, $CyMe_4$-BTBP and $CyMe_4$BTPhen which exhibit potential for the separation of minor actinides from lanthanides in the management of spent nuclear fuel, have been prepared and characterized in solution and solid state. This information is used to assess the lanthanide(III) speciation obtained when extracted into the organic phase in liquid-liquid separation conditions, probed by X-ray absorption spectroscopy.